https://ntrs.nasa.gov/search.jsp?R=19670005598 2020-03-16T18:50:16+00:00Z

TECH LIBRARY KAFB, NM
0060140
NASA CR-
c.1

NASA CONTRACTOR REPORT

NASA CR-683

LOAN COPY
AFWL
KIRTLAND

MASS SPECTROMETER ANALYSIS OF SOLID MATERIALS WITH THE ION-MICROPROBE SPUTTER SOURCE

by R. F. K. Herzog, W. P. Poschenrieder, and F. G. Satkiewicz

Prepared by
GCA CORPORATION
Bedford, Mass.
for Goddard Space Flight Center

NATIONAL AERONAUTICS AND SPACE ADMINISTRATION • WASHINGTON, D. C. • JANUARY 1967

TECH LIBRARY KAFB, NM
0060140

NASA CR-683

MASS SPECTROMETER ANALYSIS OF SOLID MATERIALS WITH THE ION-MICROPROBE SPUTTER SOURCE

By R. F. K. Herzog, W. P. Poschenrieder,
and F. G. Satkiewicz

Distribution of this report is provided in the interest of information exchange. Responsibility for the contents resides in the author or organization that prepared it.

Prepared under Contract No. NAS 5-9254 by
GCA CORPORATION
Bedford, Mass.

for Goddard Space Flight Center

NATIONAL AERONAUTICS AND SPACE ADMINISTRATION

For sale by the Clearinghouse for Federal Scientific and Technical Information
Springfield, Virginia 22151 – Price $2.00

TABLE OF CONTENTS

Title	Page
SUMMARY	1
INTRODUCTION	3
IMPROVEMENT OF THE INSTRUMENT	7
EXPERIMENTAL	13
SAMPLE PREPARATION	39

MASS SPECTROMETER ANALYSIS OF SOLID MATERIALS WITH THE ION-MICROPROBE SPUTTER SOURCE

by

Dr. R.F.K. Herzog, Dr. W.P. Poschenrieder and F.G. Satkiewicz

GCA Corporation, GCA Technology Division
Bedford, Massachusetts

SUMMARY

The Sputter Ion Source Mass Spectrometer developed by GCA Corporation under the auspices of NASA has already proved to be a valuable analytical tool. The present report describes a number of instrumental improvements, explains an important discovery about the initial energy distribution of the sputtered ions, and particularly deals with geological applications of the instrument.

Within the mechanical improvements, the introduction of the so-called "Energy Window" is of great importance. It makes use of the discovery that the initial energy distribution of atomic ions differs significantly from the energy distribution of molecular ions. When the energy window is properly set, either predominantly atomic or molecular spectra are obtained. This adds a new analytical dimension of significant value to the instrument. Very heavy molecules such as $A\ell_{18}$ can now be detected. These molecules may be regarded as microcrystalline units of the material and their composition obviously reflects the crystalline structure of the material. Thus, a new way for the structural analysis of solids is opened. A very significant and for a specific material characteristic intensity distribution of these heavy ionized fragments points to an even more sophisticated analysis of solids. These distributions obviously reflect the stability of these units and may permit basic crystallographic research applications. The enormous potential recognized here could only be touched in this phase of the contract.

Geological application was restricted to the two samples supplied by NASA. The possibility of measuring low concentration isotope ratios in the strontium and rare earth region in the complex matrix of a rock was investigated including the selection and preparation of proper fluxing agents. Although the problem imposed could not be solved completely mainly because most of this work was performed before the instrument was improved, the knowledge gained ensures that better results may be expected for the future.

INTRODUCTION

During the last decade, mass spectrometry has become a widely accepted analytical tool of high efficiency. Fast analysis on a routine basis, high accuracy, very high sensitivity for trace constituents, and small sample consumption can be listed as its advantages. The versatility of the method allows the adoption of special applications, such as the measurement of isotope ratios, the accurate determination of atomic masses, the investigation of chemical reactions, and the observation of fast changes in sample composition.

Mass spectroscopy has been particularly successful for gaseous samples. The analysis of solids, however, has not yet achieved equal success because, in most cases, the necessary vaporization and ionization of the solid material encounters many technical difficulties. If a regular electron impact ion source is used, the whole ion source has to be kept at a high temperature so that recondensation of the material evaporated from a high temperature oven can be prevented. The thermionic ion source only works well with alkaline metals and earths; therefore, it has only very limited applications. In addition, both techniques give large discrimination because the vapor pressures and the evaporation rates of the different sample constituents may vary by many orders of magnitude. The third conventional technique makes use of the spark source and, so far, has found the widest acceptance for general analytical work; in this case, a high frequency spark between the sample electrodes produces the ions. For all elements the sensitivity is fairly uniform. This permits a semi-quantitative analysis on a routine basis where an order of magnitude accuracy is sufficient. Higher accuracy can be achieved if the instrument is calibrated with a sample of accurately-known composition which, in addition, has to be similar to the sample in question. High sensitivity in the ppm range, and in special cases in the ppb range, can be reached; thus, spark source spectroscopy has become an important analytical method although a number of disadvantages have to be taken into account. Because the ion current is not stable, the source is unsuitable for a scanning spectrometer with electrical output. Additionally, a large energy spread of the ions is produced in a spark source; consequently, a double focussing mass spectrometer employing a photographic plate has to be used. Although the whole spectrum can be obtained simultaneously with the photographic plate and integration over a long time is possible, the introduction of the plate into the vacuum, the long pumpdown time of the magnet chamber of the spectrometer, the removal of the plate, the developing, and finally, the measurement of the lines with a microdensitometer are all inconvenient and time-consuming procedures. Because the photographic plates outgas, sufficiently low pressures are not easily obtained and collisions of the ion beam with the residual gas become serious. These collisions result in charge exchange and scattering effects which fog some sections of the photographic plate. In addition, a large part of the mass scale is usually covered by multiply-charged ions and molecular species of the main constituents, which the spark source abundantly produces. Also, sparking of a sample is a rather crude and destructive method and it is very difficult to select a certain spot of the sample for the analysis. Equally problematic is the examination of a thin layer of film, though recently some efforts have been made in this direction.

It was to overcome these difficulties that a new ion source for solid materials was developed and tested under the previous contracts - JPL 950118, 950576, and NASw-839. Bombardment of the test sample with an intense beam of primary ions causes rapid sputtering of the sample. Most of the sputtered particles are neutral but a fair fraction leaves the sample electrically charged. The energy distribution of the secondary positive ions depends in a complex manner on the bombarding energy, the weight and nature of the bombarding gas, the sample matrix, and the kind of ion formed. Although the energy distribution has a half-width which in all cases is only about 20 eV and peaks between 10 and 30 eV, a fair number of ions with considerably higher energy is produced. Thus, the use of a double focussing mass spectrometer becomes necessary here if high resolution and transmission are to be achieved at the same time. But, as is pointed out in this report, double focussing is not just a plain necessity in this instrument. The possibility of selecting a certain band out of the initial energy spread range provides important additional information about the nature of the sample.

A specially designed mass spectrometer serves for the analysis of the secondary ions. It utilizes a homogeneous magnetic field with curved boundaries and a modified toroidal electric field. This arrangement provides stigmatic focussing and energy focussing as well as some corrections of image errors and a smaller weight of the magnet for a given resolution and transmission. The ion beam is either collected directly or converted into an electron beam which is multiplied and recorded in the usual way.

The basic advantage of this new method over the conventional spark source mass spectrometry is that the total ion current stays practically constant, which permits scanning of the mass spectrum and direct electrical measurement of the mass peaks. The mass spectra obtained with the sputter source show, by far, fewer multiple charged ions, and molecular species can be enhanced or be suppressed deliberately, depending on the information required. Thus, simpler mass spectra are obtained and interpretation is facilitated.

The bombarding ion beam can be focussed to an area of about 0.001 cm^2 or defocussed up to 0.5 cm^2. Typical sputter rates are between 0.02 and 0.0001 cm/hour depending on the area bombarded. Thus a volume of 20×10^{-6} cm^3, or material between 10 and 400μg is consumed for a one-hour analysis. The small focus allows the instrument to be used as an "ion-microprobe" to study the distribution of any particular element in an inhomogeneous sample by moving the sample relative to the bombarding ion beam. Since the primary beam sputters away layer after layer of the sample, the change of composition with depth can be studied too.

As another important advantage of the new ion source, the sample does not require any special chemical or extensive mechanical preparation; this prevents contamination of the sample by these processes. Even cleaning of the surface can often be omitted since the contaminated surface layers are sputtered away within a few minutes and afterwards, only the bulk material is analyzed. The method is not restricted to conductive materials. Non-conducting samples may be analyzed without the addition of conducting materials such as graphite, as is necessary in spark source mass spectroscopy or optical spectroscopy. Gases, such as hydrogen, nitrogen, oxygen, chlorine, and others can also be detected readily.

However, the sputter ion source shares one problem with other methods mentioned previously, namely; discrimination. For the sputter ion source, this effect is not so much caused by the differing sputter yields of different elements which are still all within one order of magnitude, but rather by a largely varying ionization yield. This difference is still favorable insofar as fractionation is less pronounced than with other methods. Nevertheless, calibration procedures are required for a quantitative analysis.

Unfortunately and despite strong efforts by numerous investigators, the sputter mechanism is not yet too well understood. This is particularly true for the ionization effects connected with sputtering. It is hoped that in the near future an increase in knowledge will enable a semi-quantitative analysis to be made by the use of known constants such as work functions and ionization potentials which somehow seem to govern the ionization yield.

The work under this contract was aimed at the use of the instrument as a tool for geological investigations. One point of particular interest was the determination of isotopic ratios of spurious elements like the rare earths in a rock sample. Earlier work [1]* in this direction has already indicated the basic potential of the method, but for such extreme requirements, a number of improvements had to be made.

Equally important, if not contingent for the solution of the task, was and is a better understanding of the sputtering phenomena. Accordingly, work in this direction was also undertaken. An interesting and exciting new discovery was made about the energy distribution of the sputtered particles. This discovery leads to a very practical application.

Since isotope dilution techniques are frequently used in geological analysis, which requires sample preparation, part of the work also deals with this problem and the selection of a suitable flux.

However, in the limited time available for this work, still many questions are left unanswered.

Though many valuable and unique information can already be gained with the instrument, it is felt that its full potential is by far not explored and utilized and that as more work follows the application of this instrument and the appropriate techniques can be fully exploited.

---

*Numbers in [ ] throughout text indicate reference numbers.

IMPROVEMENT OF THE INSTRUMENT

In the past, not too much effort was directed toward an evaluation of the resolution of the instrument, although in an earlier experimental setup of the instrument, a resolution of 2000 at half height had been obtained, in good agreement with the theoretical expectations for the slit width then in use. Subsequently most attention was paid to high transmission and to the solution of other problems where high resolution was not needed. Therefore, the instrument was adjusted to yield a resolution of about 300 at half height. The new requirements to perform measurements in the rare earth and lead region placed more emphasis on better resolution.

The behavior of the instrument in dependence on its parameters of adjustment was tested with a special electronic method. All the secondary acceleration voltages including the deflection field voltages in the correct proportions were scanned simultaneously with the x-axis of an oscilloscope in a sawtooth-like manner. The signal from the ion-electron multiplier was amplified by a fast Keithly electrometer and given on the y-axis of the scope. The repetitive sawtooth frequency was high enough to produce a steady picture of the mass peaks on the screen of the oscilloscope. This method, which is similar to the one used for "peak matching," permits an immediate judgment of the effect of any variation of adjustment parameters. It also indicates the achieved resolving power in an easy, unambiguous manner. With this setup the spectrometer could be adjusted to yield a resolution of more than 4500 at half height under conditions which should result in a theoretical resolution of 5000. A demonstration of this resolution is given in Figure 1. During the adjustment procedures, a number of deficiencies detected were traced to the following sources.

(a) The narrow tubular connection part between the entrance slit and the magnetic field, which also contains the valve that separates the target chamber from the analyzer, has a tendency to build up wall charges. These charges distort the correct ion orbit and adversely affect the resolution. This effect strongly depends on the kind of sample and the adjustment of the secondary beam optics and is a function of time. Additional disc apertures in this section bring improvement but redesign of this section is planned.

(b) The behavior of the peaks, when the secondary optics were changed, indicated that the very wide apertures which limit the solid angle acceptance and the energy width have to be reduced somewhat in order to guarantee reproducibly high resolution. It was found that this reduction results in no appreciable intensity loss. Generally, the natural solid angle of the ion beam behind the entrance slit seems to be smaller than the one originally permitted. However, the critical center position is not sufficiently fixed by the too wide aperture.

(c) The original circuitry from which all the secondary voltages were taken was not sufficiently stable and, in particular, the deflection voltage for the condenser was not completely decoupled from the primary beam system. In addition, a considerable hum component modulated the electric deflection field and, accordingly, widened the peaks.

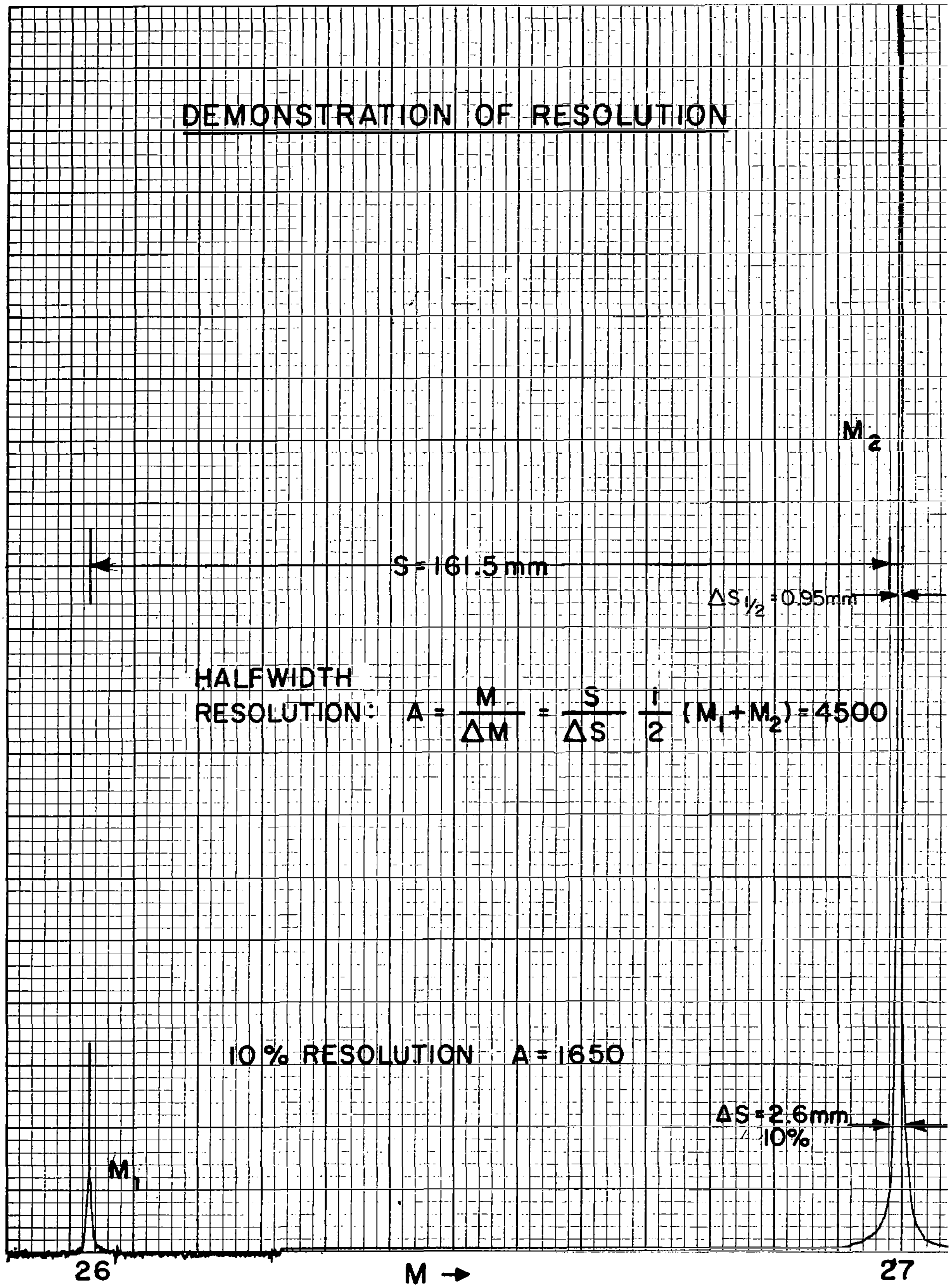
DEMONSTRATION OF RESOLUTION
M₂
S = 161.5 mm
ΔS ½ = 0.95mm
HALFWIDTH
RESOLUTION: A = M/ΔM = S/ΔS · 1/2 (M₁+M₂) = 4500
10 % RESOLUTION A = 1650
ΔS = 2.6mm
10%
M₁
26
M →
27

Figure 1

The problems encountered under (c) were eliminated by an entirely redesigned secondary voltage circuitry. The original Nuclide high voltage power supply was substituted by a Fluke power supply of higher stability (0.005 percent for 10 percent line change). The complete schematic of the new arrangement is shown in Figure 2.

Since none of the high voltage power supplies on the market provide suitable scanning of the output voltage, a scanning device was incorporated into the new additional circuitry. For this, a unique circuit utilizing a parallel regulator was designed. The maximum sweep amplitude at an acceleration voltage of 1000 V is about 400 V, which corresponds to a 40 percent sweep in the mass range. It is, therefore, possible to sweep, for instance, from M = 3 to M = 5, or from M = 6 to M = 10, or from M = 12 to M = 20, or from M = 120 to M = 200, etc. The use of a wider sweep range was not advisable because of the change in transmission, and accordingly in sensitivity, which is connected with any change of the acceleration voltage. The sweep voltage may be taken from the relaxation generator which is an integrated part of the circuitry. Sweep frequencies between ca 0.02 and 100 Hertz are available. The sweep voltage can also be monitored by an external voltage. Coupling with this voltage is dc; thus, programming of the acceleration voltage is not restricted by any low frequency limit. A programming voltage between ±7 volts will utilize the full sweep range of the acceleration voltage. By proper adjustment of the workpoint of the circuitry with trimpot T_1 (see schematic Figure 2), the full sweep range may also be attained with external monitoring voltages, which range from 0 to +14 volts or also from 0 to -14 volts. Thus, versatility is provided. Adaption to the digital memory oscilloscope is very simple with the new unit. The Northern Scientific NS513 Memory Oscilloscope, which is best suited for the application here, delivers an external time base voltage from 0 to 9 volts, which sweeps the acceleration voltage by 250 volts, and accordingly the mass range by 25 percent. The feedback feature of the new sweeping unit guarantees that the acceleration voltage follows the monitoring signal with high accuracy, maintaining the correct proportionality between input and output signals. The absolute acceleration voltage is selected on the Fluke high voltage power supply. The sweep unit will also follow this voltage change proportionally.

Complete decoupling between both branches is achieved. In addition, the voltages for the suppressor and the multiplier grid, which previously were taken from batteries, are now obtained from the same circuitry. Two separate voltage dividers are used for the condenser voltages and for the remaining voltages divider for the condenser uses wire wound precision resistors and is completely shielded. Hum on the condenser field is now negligible.

Another new and important feature is the "Energy Window" adjustment. The target potential can be varied independently from all other secondary voltages. The consequences of this setting are discussed below along with the details of the experimental arrangements.

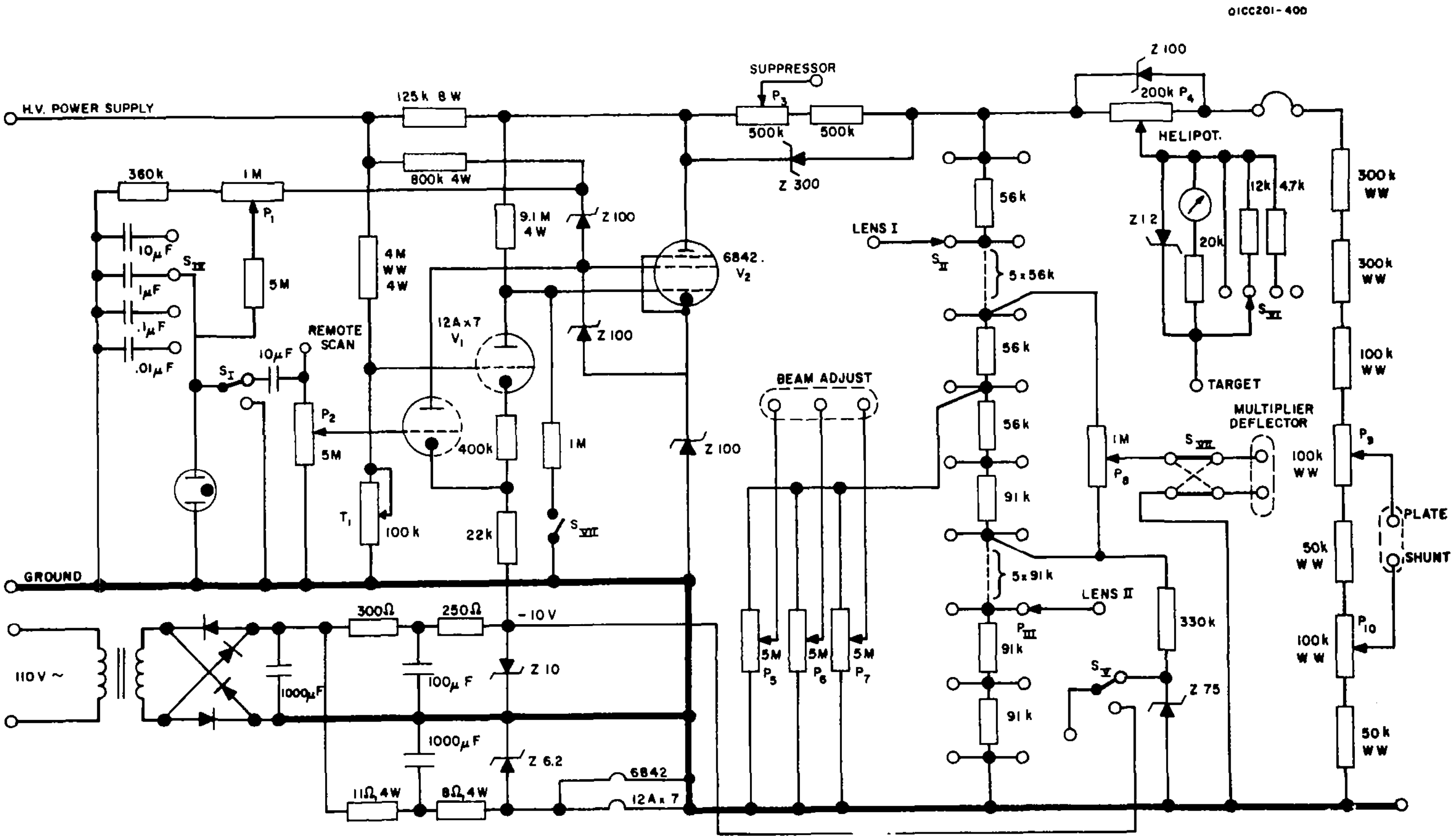
01CC201-400
H.V. POWER SUPPLY
125k 8W
800k 4W
360k
1M
P_1
5M
10μF
1μF
.1μF
.01μF
S_{IX}
S_I
10μF
REMOTE SCAN
P_2
5M
4M WW 4W
T_1
100k
12A×7 V_1
9.1M 4W
400k
22k
1M
S_{VII}
Z 100
Z 100
Z 100
6842. V_2
GROUND
110V ~
300Ω
250Ω
-10V
1000μF
100μF
1000μF
Z 10
Z 6.2
11Ω 4W
8Ω 4W
6842
12A×7
SUPPRESSOR
P_3
500k
500k
Z 300
56k
LENS I
S_{II}
5×56k
56k
56k
91k
5×91k
LENS II
P_{III}
91k
91k
BEAM ADJUST
5M P_5
5M P_6
5M P_7
1M
P_8
330k
S_V
Z 75
Z 100
200k P_4
HELIPOT.
Z 12
20k
12k
4.7k
S_{VI}
TARGET
MULTIPLIER DEFLECTOR
S_{VIII}
300k WW
300k WW
100k WW
100k WW
P_9
50k WW
100k WW
P_{10}
50k WW
PLATE
SHUNT

Figure 2. Secondary voltage circuitry schematic.

The multiplier contains a grid between the last dynode and the collector which serves to reverse the originally negative output signal to positive. A positive signal is required for the logarithmic range of the electrometer. This grid was previously biased at +40 volts to achieve the change in signal polarity. The multiplier grid voltage was increased to 75 volts, because better multiplier linearity is obtained, particularly for higher multiplier output signals. Also, a switch was incorporated with which the multiplier grid may be set at -10 volts. This setting produces a negative output signal and results in an about 3 times higher multiplier amplification. Highest linearity is maintained under this condition together with the linear range which is recommended for high precision isotope ratio measurements.

A microammeter now reads the target current directly, which is very helpful for the primary beam adjustment and for monitoring the primary beam stability.

With an external defocusing arrangement for the primary beam, a further improvement in instrument versatility was achieved. A similar arrangement had been used in an earlier phase in the development of the instrument; however, it had been abandoned because of deficiencies in the former einzellens arrangement. This time, with some alterations in the structure of the einzellens of the duoplasmatron, the device proved very successful. In contrast to the earlier design, the variable center electrode draws only a very negligible electron current and no increase in flashover was observed. Therefore, a simple additional voltage divider, incorporated into the already existing one, was sufficient. With this focus adjustment, the bombarding spot on the sample can be varied from 0.3 to 7 mm diam. The lower diameter is limited by the space charge and the upper diameter by the width of some apertures in the primary beam system. A very homogeneous sputter rate is now obtained with the defocused beam. This is of importance for the measurement of concentration gradients and for thin film analysis. The defocused beam also permits the averaging of the composition of a sample over a larger area.

Additional improvement of instrument performance was achieved by the applecation of a special magnetic shunt to the duoplasmatron and by magnetic shielding of the acceleration and focussing region of the secondary beam system in front of the entrance slit. Previously, a magnetic stray field from the strong duoplasmatron magnet had caused a mass selection between target and entrance slit which resulted in some mass discrimination. This discrimination became particularly serious when ions with low initial energy were used. Now, this effect is practically negligible.

Unfortunately, and due to delayed delivery dates, we were not able to bring another very important improvement to an experimental state within this contract period. This consists in the addition of a hot filament to the present target structure. The function of this filament is to eliminate serious charge-up effects which can and do occur with insulating samples. Charge-up of the sample does not only result in instabilities of the beam intensities and focusing conditions, but also changes the originally selected energy range in an uncontrolled way, as will be explained later. This can be particularly detrimental if isotopic ratios are measured by scanning the acceleration voltage. The filament which will be close to the sample surface will be kept at a slightly negative potential with respect to the target potential. If the surface is charging up more positively by the impinging ions, more electrons will flow to the surface and automatically compensate for the charge-up. Thus, the surface potential will always be only slightly above the filament potential. Since the filament is working on a high and sensitive potential, a special insulation transformer with shields is required. Also, in order that interference modulation of the beams by ac may be avoided, the filament has to be heated by dc.

It is also expected that the injection of electrons into the primary beam near to the focus will result in an even sharper focus due to the compensation of the space charge within the primary beam itself.

EXPERIMENTAL

The Initial Energy Distribution of Sputtered Ions and the Intensity Distribution of Heavy Molecular Ions

Certainly the most important discovery with the greatest potential was made by a systematic investigation of the distribution of the initial energy with which secondary ions are formed by the sputtering process. Information about this phenomenon in the literature is only sparse and contradictory and theory is not developed to a point that allows any conclusions. Generally, it is assumed that the initial energy spread is limited to small energies up to a few ten electron volts.

Since the mass spectrometer used together with the sputter ion source is a double focussing instrument, it is comparatively easy to determine initial energy distributions. To enable this measurement, it is necessary to reduce the apertures which determine the width of the transmitted energy range and to change the ratio between electrical deflection and acceleration voltage. The apertures were accordingly reduced to transmit only an energy band of 4 eV in width. For convenience, the deflection voltage was kept constant to preserve the scale and only the acceleration voltage - in this case given by the target potential - was changed.

The working principle may be explained in the following way: The ion orbit is determined by the position of the fixed slits in the mass spectrometer. Therefore, only ions of a certain energy will be able to pass through the electrostatic analyzer (condenser) and through the exit slit. This energy depends solely on the electric deflection field, that is, the voltage applied to the condenser. Say, this voltage is chosen to pass ions with an energy of 998 to 1002 eV; then, the initial energy which ions must have in order to pass is given by the difference between 1000 ± 2 V and the actual target potential. For example, if the target voltage is 900 volts, ions will gain an energy of 900 eV by falling through the acceleration potential but must have an additional initial energy of 98 to 102 eV to be transmitted through the mass spectrometer.

Earlier experiments had already indicated significant changes in the appearance of the spectra depending on the adjustment of the transmitted energy range. The systematical work initiated under this contract shed light onto this and other phenomena which were not understood before.

Figure 3 shows the energy distribution for the different ions obtained from an aluminum wire with a 5 percent magnesium content under bombardment with 12 keV argon ions. Some remarkable observations can be made.

(a) All sputtered ions have a pronounced maximum for energies between 10 and 30 eV. The position of the maximum is slightly different for atomic and molecular ions, with the latter peaking at lower energy.

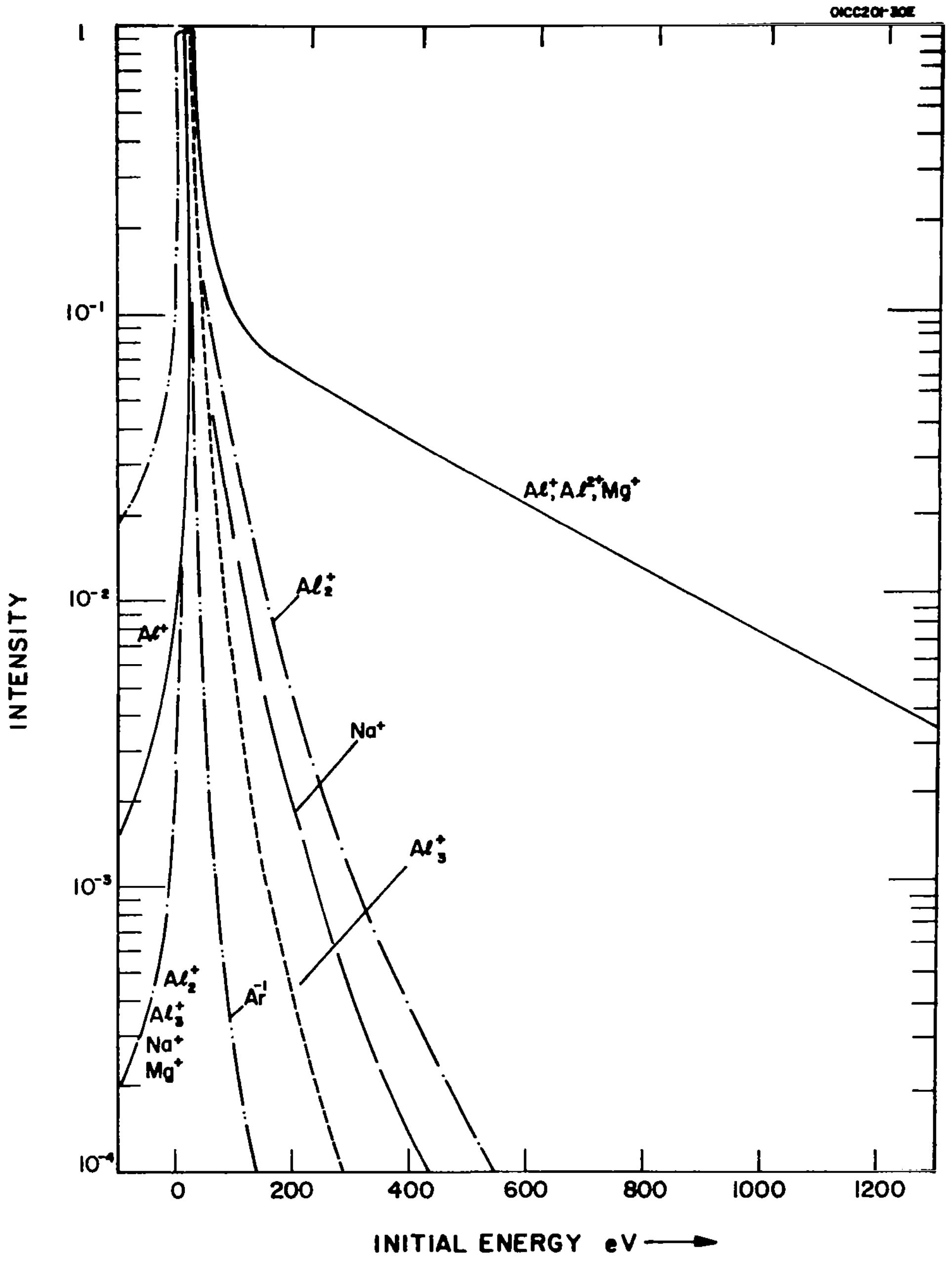

Figure 3. Energy distribution of $A\ell^+$, $A\ell^{2+}$, $A\ell_2^+$, $A\ell_3^+$, Mg^+, Na^+, Ar^+ sputtered from an $A\ell$-Mg-alloy with 12 KeV Ar^+. (All intensities normalized to "one".

(b) Most significant is the slow drop-off in intensity for atomic ions with high initial energies. In contrast, molecular species show a sharp drop-off which becomes increasingly sharper with the number of atoms in the molecule.

(c) Multiple charged ions behave mainly like singly charged atomic ions with regard to the energy distribution.

(d) The measurements show a number of ions with "negative energies." These must be ions which are formed from free neutrals close to the surface, obviously by electron impact from secondary electrons or by interaction with the primary beam. Since they are formed on a potential lower than the target potential, and by definition of our zero point, they appear to have negative energies.

(e) The energy distribution of the secondary Ar^+ is positioned at very low energy with a fair amount of "negative energies." To some extent, this may be explained by the concentration of Ar around the target and the same mechanism as under (d).

(f) Na^+ in this sample behaves like the molecules with regard to its energy distribution. This might be typical for a surface contaminant. The sodium peak decreased considerably with prolonged sputter time, which supports this assumption. In contrast, Mg^+ behaves exactly like $A\ell^+$.

The influence of a different setting of the energy window on the spectra is demonstrated in Figures 4 and 5. Figure 4 shows a spectra as obtained with a setting which transmits only ions with an initial energy between 350 and 300 eV. This adjustment was generally used in the past. The spectrum was obtained from the same Aℓ Mg alloy as was used for the energy distribution measurements above and shows essentially atomic ionic species. In strong contrast, the spectrum of Figure 5 is very rich in molecular ions. At first sight, it is hard to believe that both spectra have been obtained from the same material, but here the energy window was adjusted for the maximum in the energy distribution. From a comparison of both spectra, the following conclusions may be drawn.

(1) If the energy window is set to look at the energy of optimal intensity, heavy molecular ions of all possible combinations of the constituents are well recognizable in the spectra; thus, some resemblance to spark spectra is shown.

(2) Setting of the energy window to an initial energy of about 300 eV results in an intensity loss for the atomic peaks of a factor of 50, but $A\ell_2$ is reduced by three orders of magnitude and higher molecules are below the detection limit.

(3) The adjustment for the molecular spectrum, also shows a general enhancement of elements like sodium and potassium. This is particularly obvious during the initial sputter period as long as the surfaces are not cleaned by the sputtering beam. Vice versa, one comes to the conclusion that the high energetic ions are more representative for the bulk composition.

The same measurements and comparisons were made with Si and Pt. Silicon was quite similar to aluminum in its relevant behavior and therefore, can be omitted from detailed reporting.

Platinum, however, gave a different picture. The energy distribution of the atomic Pt dropped off at the high energy side at a much higher rate (Figure 6). Molecular ions of platinum were not measured, because they were beyond the mass range which can be scanned with 1000 eV acceleration voltage. The behavior of the contaminants Ca and Na in this sample seems somewhat peculiar. It is known from an earlier analysis that this sample contains only very little Na in the bulk. The Ca peak, however, is a main bulk contaminant yielding a peak about equal to Pt, in contrast to the fact that the sample is supposed to be high purity (0.999999) platinum [2]. This indicates a strong discrimination effect since other detection methods suggest a concentration of Ca in the 1000 ppm (!) range. A full spectrum of the platinum sample, run with the energy window set at the maximum of the energy distribution, is given in Figure 7. Comparison with our earlier spectrum [2] shows much resemblance, though some molecular species are more obvious now, and the intensity ratios of some contaminants appear changed. But the striking difference, pointed out previously in the case of Aℓ, is not observed. The interpretation of some molecular peaks is tentative and seems to indicate that oxides of Aℓ, Ca, and Zr form microcrystalline inclusions. The origin of these contaminants may be traced to the use of a zirconia crucible for the manufacturing process.

Theoretical considerations suggest that part of the differences between Aℓ and Pt might be due to the very different mass ratio of the bombarding gas Ar to Aℓ and Pt. To this comes the depth of penetration which depends on the ionic radius and the energy of the bombarding gas and on the transparence of the target material. The deeper the penetration and the more the collisions occur in deeper layers, the more atomic ions representative of the bulk material will be produced. This happens at the expense of the molecular ions which are too big to travel at any length through the lattice and, therefore, can only originate from the surface. The effect of the different mass ratios is more difficult to predict. As long as the mass ratio of impinging ion-to-target atoms is very different from one, little energy exchange can be expected. If the bombarding ion is lighter, it will be reflected backwards; if it is heavier it will rather drive the striken atom deeper into the bulk. Therefore, some authors [3,4] assume a different sputtering mechanism for each regime.

Since the differentiation between molecular and atomic ions is of major interest for the application of the instrument in geology, more systematic studies of the effects of the bombardment with ions of different weight and energy was advised.

At first, 12 kV He^+ ions were used on the Aℓ-Mg alloy and the energy distribution was measured as before. However, it turned out that the He was badly contaminated with hydrocarbons. In addition, a piece of indium from the seals had fallen into the duoplasmatron and produced a strong indium peak in the primary beam. Therefore, the data are questionable and it is preferred not to report them in detail before the experiment is repeated under clean conditions.

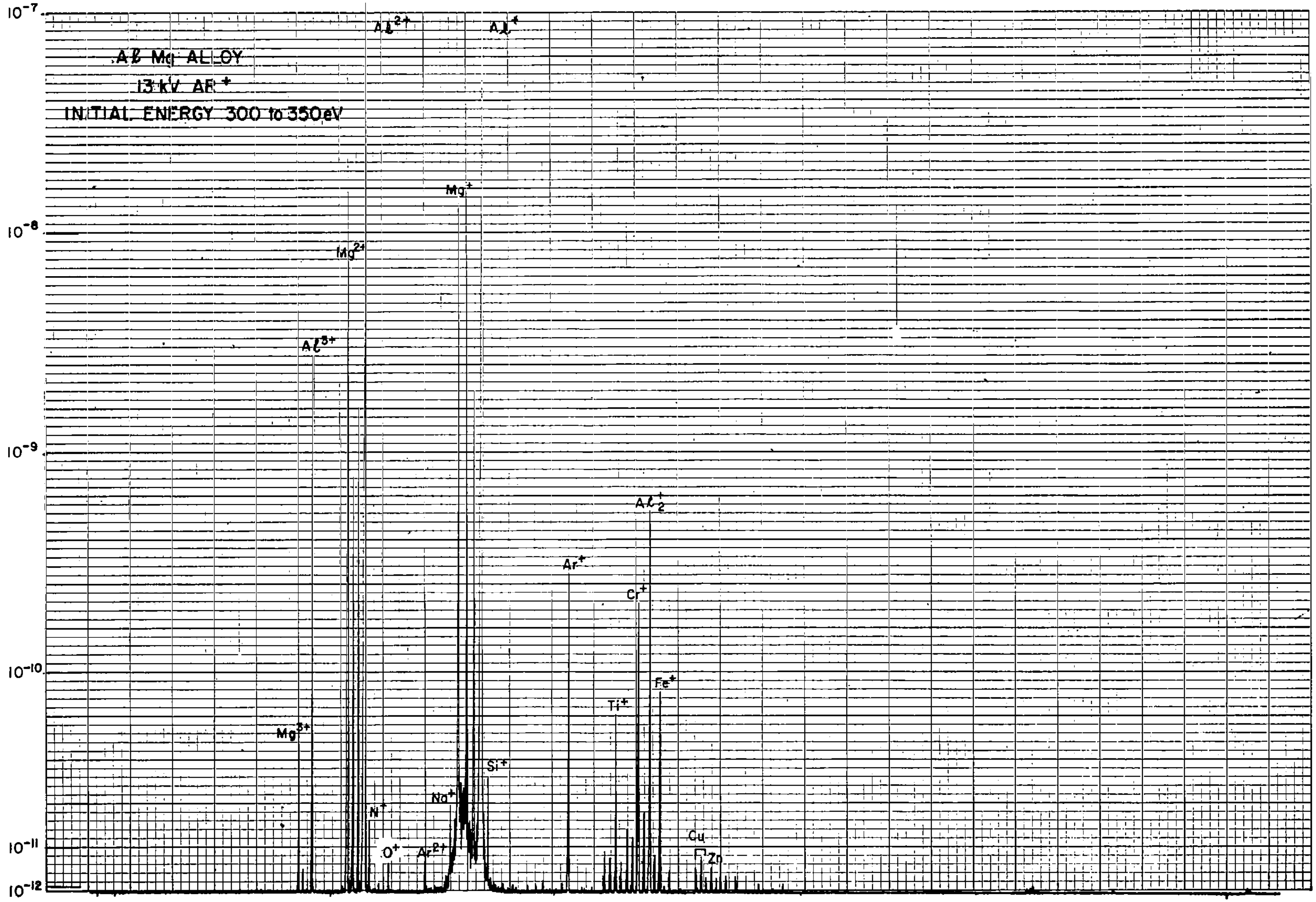
Aℓ Mg ALLOY
13 kV Ar$^+$
INITIAL ENERGY 300 to 350 eV
10^{-7}
10^{-8}
10^{-9}
10^{-10}
10^{-11}
10^{-12}
Aℓ$^{2+}$
Aℓ$^+$
Mg$^+$
Mg^{2+}
Aℓ$^{3+}$
Aℓ$_2^+$
Ar$^+$
Cr$^+$
Fe$^+$
Ti$^+$
Mg^{3+}
Si$^+$
Na$^+$
N$^+$
O$^+$
Ar^{2+}
Cu
Zn

Figure 4

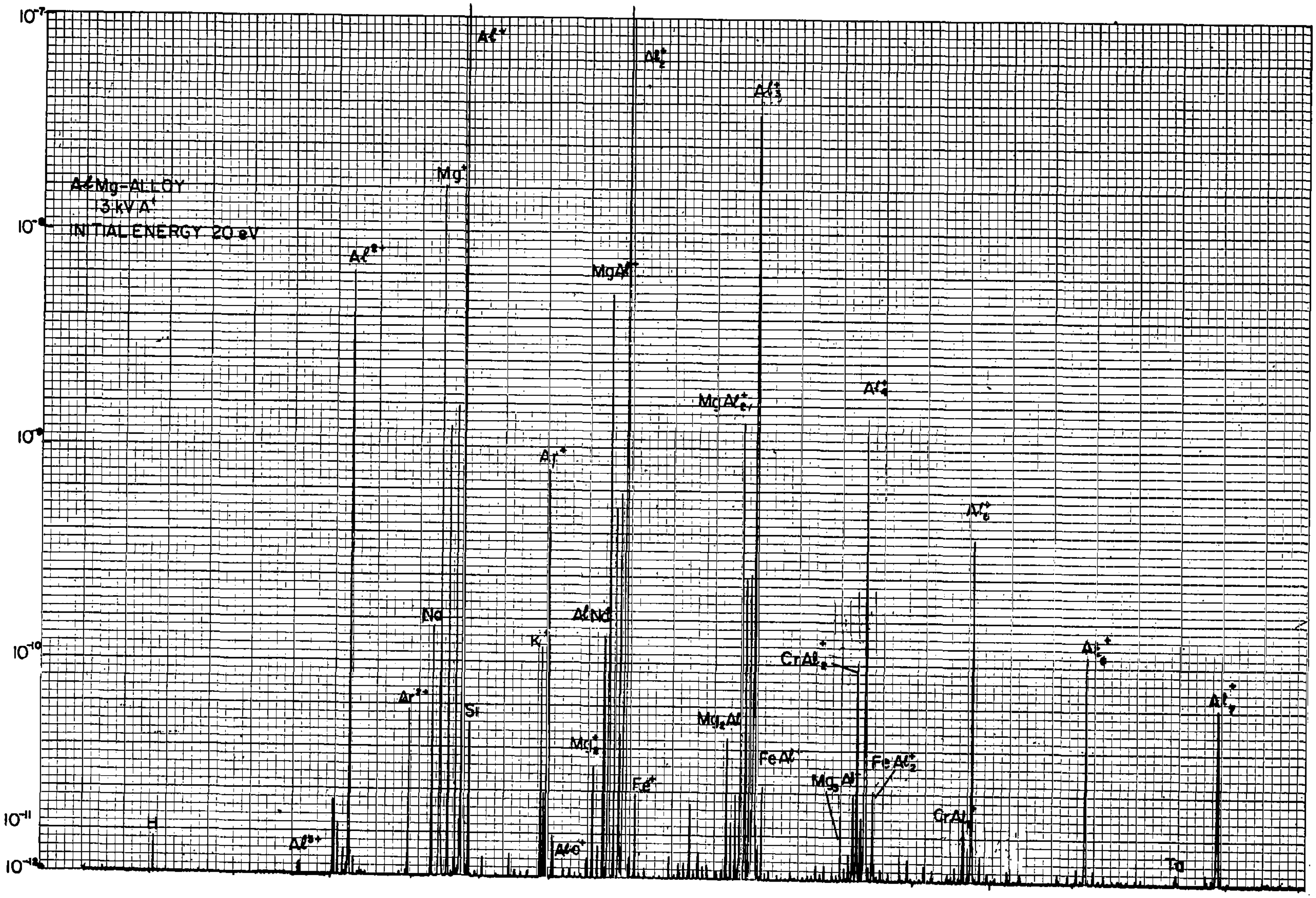
10^-7
10^-8
10^-9
10^-10
10^-11
10^-12
AlMg-ALLOY
3 kV A+
INITIAL ENERGY 20 eV
Al+
Al2+
Al3+
Mg+
Al2+
MgAl+
MgAl2+
Al4+
Ar+
Al5+
Na
AlNa+
K+
CrAl2+
Al6+
Ar2+
Si
Mg2Al+
Al7+
Mg2+
FeAl+
FeAl2+
Fe+
Mg3Al+
CrAl+
H
Al3+
AlC+
Ta

Figure 5

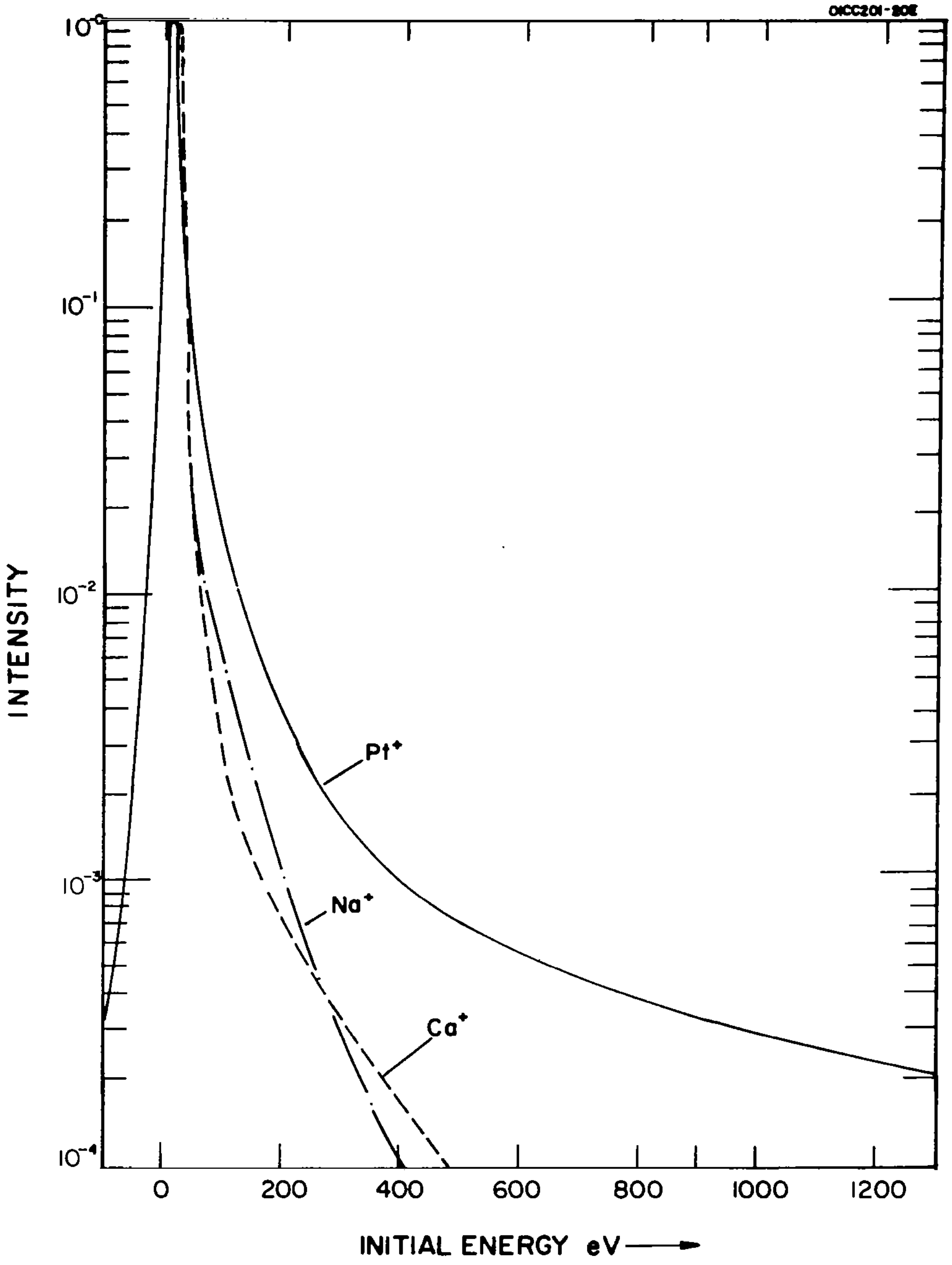

Figure 6. Energy distribution of Pt^+, Ca^+, and Na^+ sputtered from a platinum ingot with 12 KeV Ar^+. (All intensities normalized to "one".

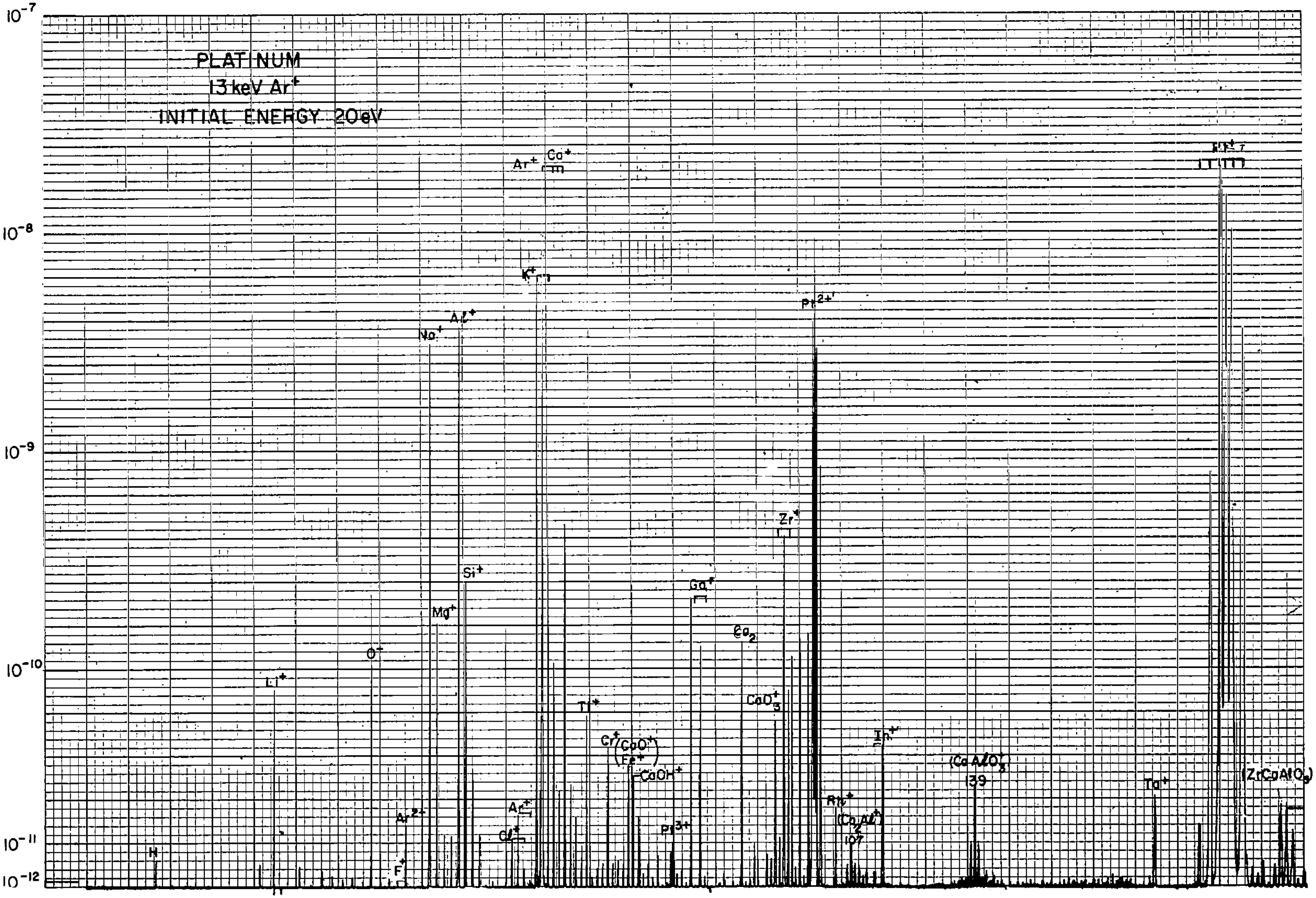
PLATINUM
13 keV Ar⁺
INITIAL ENERGY 20eV
10⁻⁷
10⁻⁸
10⁻⁹
10⁻¹⁰
10⁻¹¹
10⁻¹²
H
Li⁺
O⁻
F⁺
Ar²⁺
Na⁺
Mg⁺
Al⁺
Si⁺
Ar⁺
Ca⁺
K⁺
Cl⁺
Ar⁺
Ti⁺
Cr⁺
(CaO⁺, Fe⁺)
CaOH⁺
Pt³⁺
Ga⁺
Ca₂
CaO₃⁺
Zr⁺
Pt²⁺
Rh⁺
(Ca₂Al)⁺
107
In⁺
(CaAlO₃)⁺
139
Ta⁺
Pt⁺
(ZrCaAlO₃)

Figure 7

But it seems permissible to state that He produces less molecular Aℓ ions than Ar, in agreement with theoretical expectations.

The use of Xe for a bombarding gas was more successful. Figure 8 shows the energy distribution for the Aℓ-Mg alloy. The general resemblance with the distribution obtained with Ar (Figure 3) is obvious. It indicates a phenomenon which is more typical for the target material than for the bombarding gas. If the energy of a collision is above a certain value, a heavier molecule is fragmentated; therefore, heavy molecules do not appear with initial energies higher than this value, and the binding energies of those molecules should be somehow reflected in the energy distribution. This assumption gains further support by an investigation of the full spectrum of the Aℓ-Mg alloy given in Figure 9. This spectrum was run with a reduced acceleration voltage of 500 volts which extends the mass range to about M = 500. An interesting discovery can be made which was not so obvious when Ar was used for sputtering. Heavy molecules up to $\mathrm{A}\ell_{18}$ are visible, but they also show a puzzling structure in their intensity distribution. There is not a steady decrease in intensity with molecular weight, but a certain grouping with remarkable discontinuities is observed. From $\mathrm{A}\ell_1^+$ to $\mathrm{A}\ell_3^+$ an approximately exponential drop in intensity is seen; then a sharper drop follows with again a roughly exponential decrease from $\mathrm{A}\ell_4$ to $\mathrm{A}\ell_6$. After $\mathrm{A}\ell_7$, which is more intense then $\mathrm{A}\ell_6$, a sharper drop occurs again and a group of almost equal intensities is observed from $\mathrm{A}\ell_8$ to $\mathrm{A}\ell_{14}$ with $\mathrm{A}\ell_9^+$ and $\mathrm{A}\ell_{14}$ somewhat more prominent. From $\mathrm{A}\ell_{15}$ to $\mathrm{A}\ell_{18}$ follows another group of about equal but again weaker intensities.

Comparison with spectra from the same material but sputtered with Ar also reveals the dissimilarities caused by the use of either Xe or Ar. Up to $\mathrm{A}\ell_6$ the intensity distribution of the Aℓ-molecules is similar with the exception of a slight enhancement of the heavier molecular species. The discontinuity of $\mathrm{A}\ell_7$ is not observed with Ar and the group from $\mathrm{A}\ell_8$ on is barely detected. This difference might be explained by the poor energy exchange factor for a collision between Ar^+ and a heavy mass molecule. The general enhancement of the molecules in the case of Xe is in agreement with the assumption of a lesser depth penetration for Xe^+.

For the specific check of these results a spectrum of a pure Aℓ sample was made under the same conditions and yielded an identical result. From this it can be concluded that the observed intensity distribution of the Aℓ molecules is at least typical for aluminum. Small additions in the percent range of other elements like Mg do not affect the gross picture. As a result it may be suspected that this picture reflects the structural stability and binding forces of these heavy molecules which may be well regarded as elementary crystalline units. A rough estimate shows that these molecules are not formed out of already sputtered single atoms, but are knocked off as a whole unit. Therefore, the composition of these molecules should also indicate the basic structure of a more complex material like a silicate. This obviously opens a wide field for furture investigations.

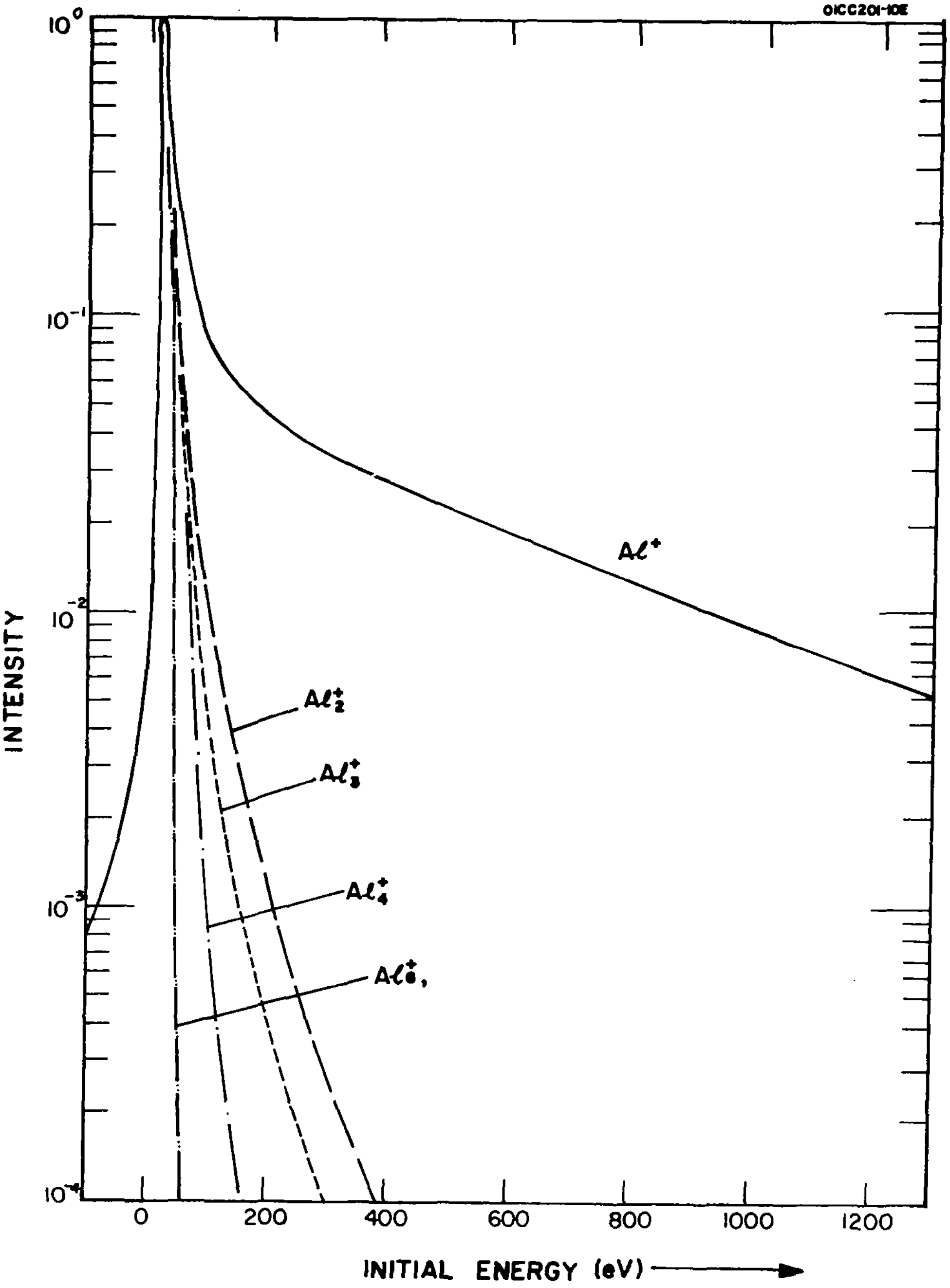

Figure 8. Energy distribution of $A\ell^+$, $A\ell_2^+$, $A\ell_3^+$, $A\ell_4^+$, and $A\ell_6^+$ sputtered from an Aℓ-Mg-alloy with 12 KeV Xe. All intensities normalized to "one".

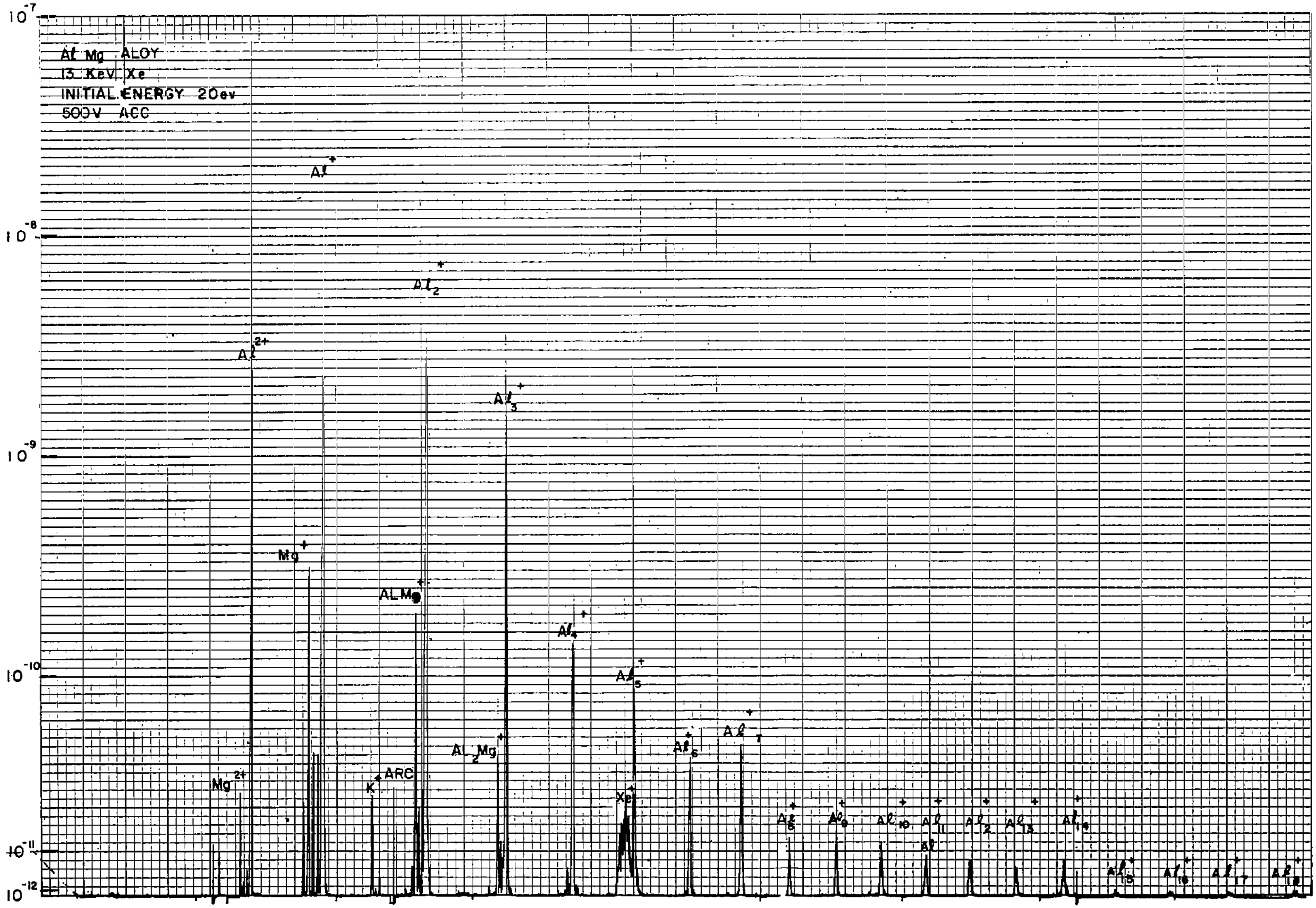
10^{-7}
10^{-8}
10^{-9}
10^{-10}
10^{-11}
10^{-12}
Al Mg ALOY
13 KeV Xe
INITIAL ENERGY 20ev
500V ACC
Al^+
Al_2^+
Al^{2+}
Al_3^+
Mg^+
$ALMg^+$
Al_4^+
Al_5^+
Al_2Mg^+
Al_6^+
Al_7^+
Mg^{2+}
K^+
ARC
Xe^+
Al_8^+
Al_9^+
Al_{10}^+
Al_{11}^+
Al
Al_{12}^+
Al_{13}^+
Al_{14}^+
Al_{15}^+
Al_{16}^+
Al_{17}^+
Al_{18}^+

Figure 9

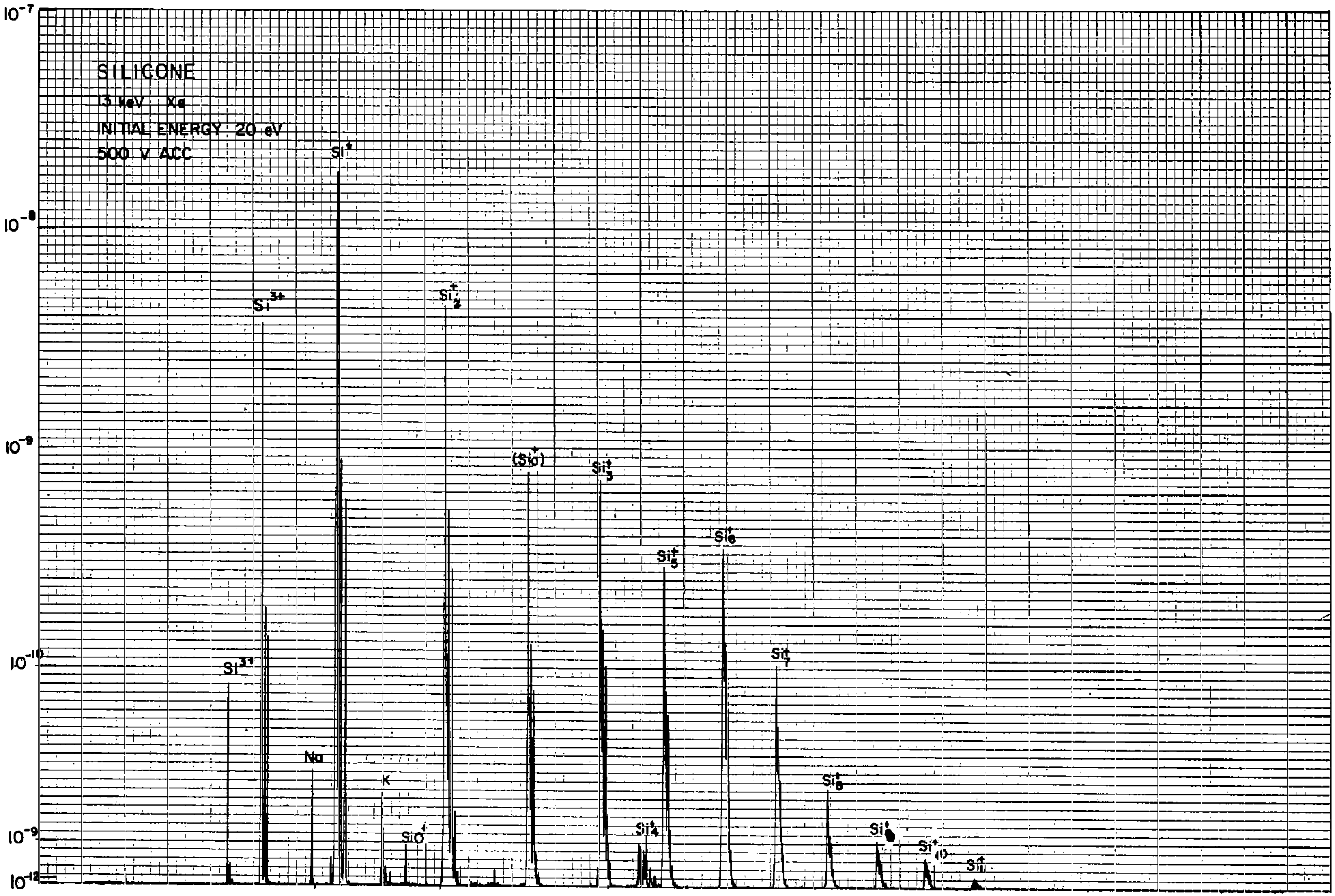
SILICONE
13 keV Xe
INITIAL ENERGY 20 eV
500 V ACC
10^{-7}
10^{-8}
10^{-9}
10^{-10}
10^{-9}
10^{-12}
Si^{+}
Si^{3+}
Si_2^{+}
(SiO^{+})
Si_3^{+}
Si_6^{+}
Si_5^{+}
Si_7^{+}
Si^{3+}
Na
K
SiO^{+}
Si_4^{+}
Si_8^{+}
Si_9^{+}
Si_{10}^{+}
Si_{11}^{+}

Figure 10

There is an astounding difference in the intensity distribution of molecular ions for materials as closely related to Aℓ as Si and Mg. Silicon in Figure 10 shows Si_3^+ and Si_4^+ almost equal in height and Si_6^+ stronger than Si_5. Above Si_{11}^+ no heavier molecule was detected. Magnesium in Figure 11 shows only Mg_2^+ and some Mg_2O^+ as molecules.

One remark should be made at this point: since the sputter process produces ionized molecules - or better, fragments - from the solid material, one must not only expect peaks corresponding to known chemical formulae which simply stand for the stycheometric composition of the material. Apart from the fact that we deal only with the ionized particles sputtered off from the sample, the intensity of a certain peak is rather a criterion for the stability of the respective crystalline unit knocked out from the structure of the solids and of the binding energy of this unit to the bulk of the sample. Nevertheless, the overall picture should give sufficient indications for the stycheometry of the sample.

Because of the rather limited funds and time of this contract, the dependence of energy and intensity distribution of molecular ions as a function of the energy of the primary beam could only be grazed. When the Aℓ-Mg alloy was bombarded with 4 keV Xe^+, and the energy window was adjusted to the maximum of the energy distribution, a considerable discrimination between atomic Mg and Aℓ was observed. Also remarkable was the fact that the $A\ell\text{-}Mg^+$ molecule had much more intensity than Mg^+. An indication of the great stability of the Aℓ-Mg molecule is also shown in Figure 9, which shows that the intensity drop between Mg^+ and $A\ell\ Mg^+$ is smaller than between $A\ell^+$ and $A\ell_2^+$.

It may be stated that these preliminary results open a new field for an application of the solids mass spectrometer in studies of structural composition of solids and in crystallography.

The Analysis of Geological Samples

Description of Samples - The National Aeronautics and Space Administration supplied two samples for the analysis.

Sample I was made from a mixture of 40 percent rock and 60 percent lithium tetraborate ($Li_2\ B_4\ O_7$). The major element composition of the rock was given as

SiO_2	52.7 percent
$A\ell_2O_3$	15.7 percent
Fe_2O_3	2.3 percent
FeO	9.0 percent
CaO	11.1 percent
MgO	6.9 percent
Na_2O	2.3 percent
K_2O	0.8 percent

Of particular interest were the elements Rb, Sr, the rare earths from La to Lu and Pb. The concentrations of these elements were given as:

Rb ~ 20 ppm

Sr ~ 200 ppm

Rare earths between
20 ppm (Ce) and 0.3 ppm (Lu)

Pb - between 1 and 10 ppm

In addition, the natural isotopic ratio of Rb and Sr had been changed by spiking the sample with Sr and Rb which contained enriched isotopes.

Sample II was derived from the same rock material, but instead of fusing the sample with a flux, the rock was dissolved in HF. After evaporation of the solution, the remaining powder was compressed to a pellet. In this case, no enrichment of Sr and Rb isotopes was performed.

General Analysis - Good spectra were obtained from both samples as shown in Figures 12 and 13, although the reproducibility of these spectra was limited. Sometimes molecular ion peaks were very strong; at other times, the spectra showed predominantly atomic ions. In addition, the ratio of the main atomic peaks kept changing. Originally all this was attributed to inhomogeneities of the samples. Later, the systematic investigation of the initial energy distribution, showed that at least part of the lack in reproducibility was owing to surface charge effects caused by the insulating nature of these samples. At this time, the instrument was adjusted for an initial ion energy of ≈ 250 eV which should mainly produce the atomic spectrum. But as soon as the surface of a sample is charged up above the adjusted potential of the target holder, through the bombardment with positive ions, the transmitted initial energy range is shifted toward lower energies. Accordingly, the more positive the surface of the sample became, the more molecular the spectra appeared.

The amount of positive charge-up depends intricately on sample nature, adjustment of the primary beam, nature of bombarding gas, history, and target holder potential. The fact that any compensation and limitation of the charge-up was at all possible is explained by an abundant amount of secondary electrons produced in the close vicinity of the target holder by the primary and secondary ion beam. These secondary electrons are released from surfaces which are on ground potential and are accelerated toward the positive target. Unfortunately, this flow of secondary electrons with high energy is not suited to produce well controlled surface charge conditions. The addition of a hot filament, a modification discussed above, however, will eliminate this problem.

The Stability of the Sputter Ion Source - One of the pre-conditions for an accurate isotope ratio determination is a reasonably stable signal. Figure 14 demonstrates the stability which could be obtained with Sample I. Since the hot filament arrangement mentioned above, was not yet installed, a very careful adjustment was required. Obviously, a well compensated surface charge condition

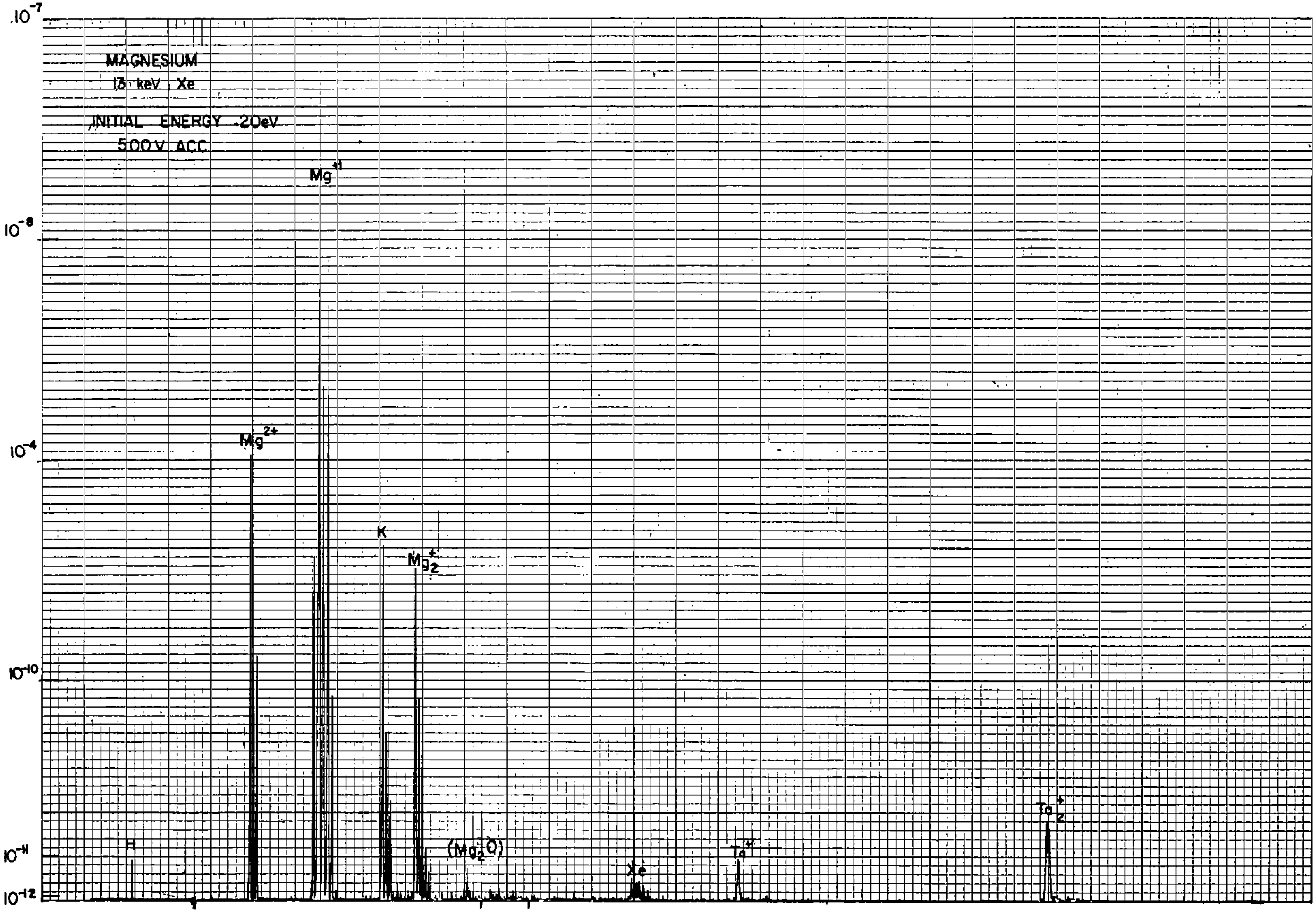
MAGNESIUM
13 keV Xe
INITIAL ENERGY -20eV
500V ACC
10^-7
10^-8
10^-4
10^-10
10^-11
10^-12
Mg+1
Mg2+
K
Mg2+
(Mg2O)
H
Xe
Ta+
Ta2+

Figure 11

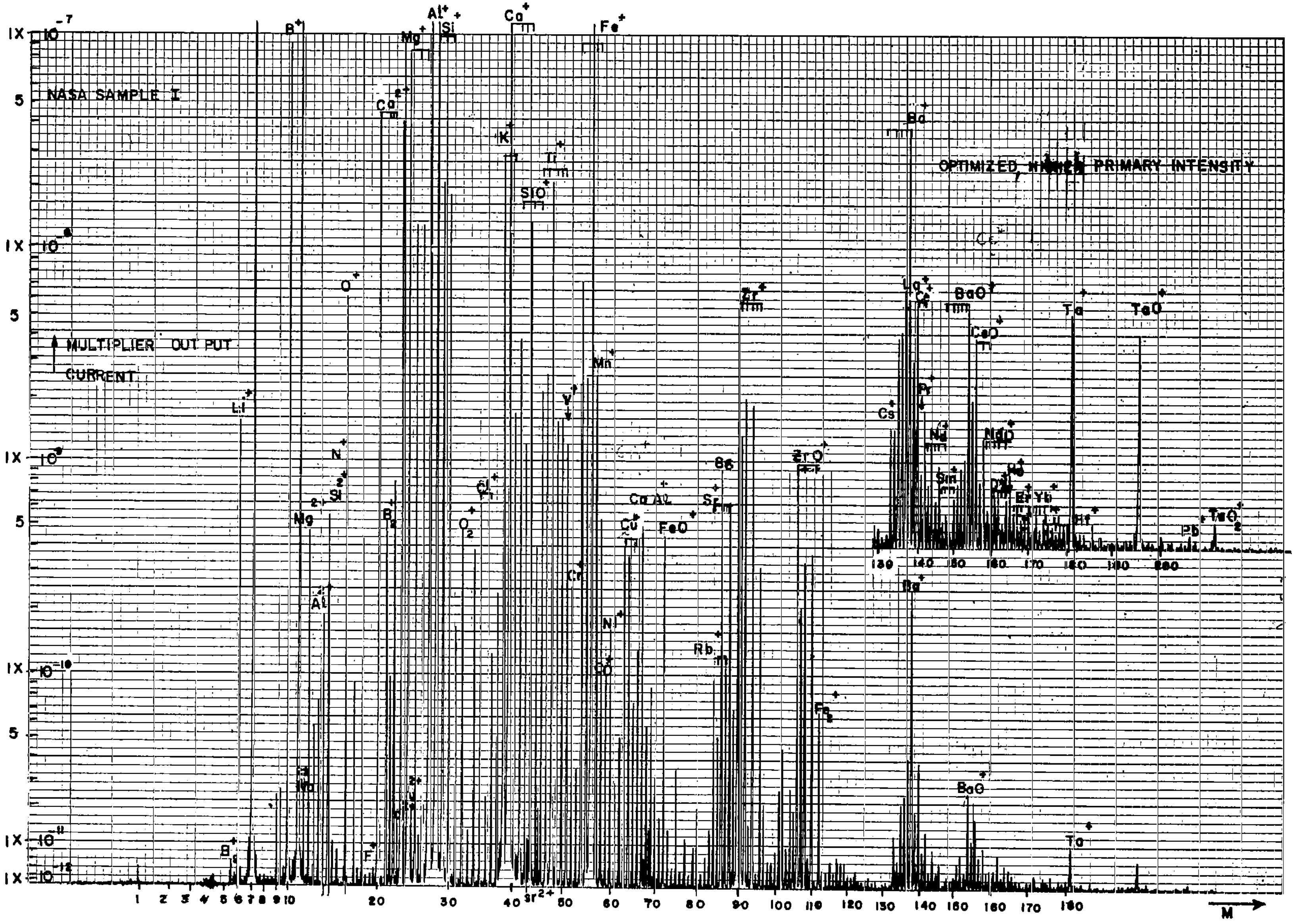
NASA SAMPLE I
MULTIPLIER OUT PUT CURRENT
OPTIMIZED PRIMARY INTENSITY
1X 10⁻⁷
5
1X 10⁻⁸
5
1X 10⁻⁹
5
1X 10⁻¹⁰
5
1X 10⁻¹¹
1X 10⁻¹²
B⁺
Al⁺
Si⁺
Mg⁺
Ca⁺
Fe⁺
Ca²⁺
K⁺
Ti⁺
SiO⁺
O⁺
Li⁺
N⁺
Si²⁺
Mg²⁺
B₂⁺
O₂⁺
Cl⁺
Al²⁺
V⁺
Mn⁺
Cr⁺
Ni⁺
Co⁺
Cu⁺
CaAl⁺
FeO⁺
Sr⁺
Rb⁺
Zr⁺
ZrO⁺
Fe₂⁺
B₂⁺
F⁺
Ba⁺
BaO⁺
Ta⁺
Cs⁺
La⁺
Ce⁺
Pr⁺
Nd⁺
Sm⁺
CeO⁺
NdO⁺
Gd⁺
Dy⁺
Er⁺
Yb⁺
Lu⁺
Hf⁺
TaO⁺
Pb⁺
TaO₂⁺
Sr²⁺
1 2 3 4 5 6 7 8 9 10 20 30 40 50 60 70 80 90 100 110 120 130 140 150 160 170 180
130 140 150 160 170 180 190 200
M

Figure 12

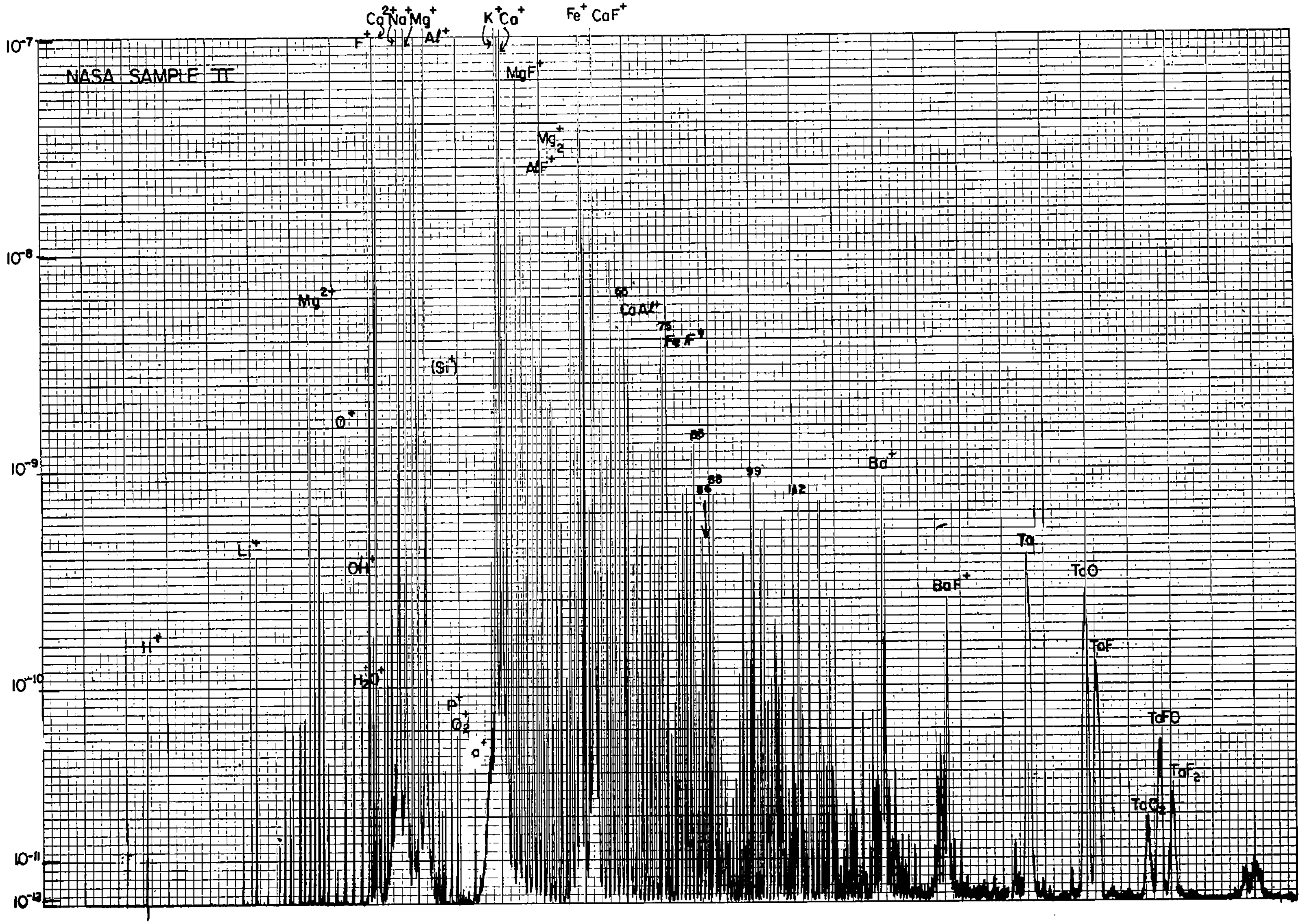
NASA SAMPLE II
10-7
10-8
10-9
10-10
10-11
10-12
F+
Ca2+
Na+
Mg+
Al+
K+
Ca+
Fe+
CaF+
MgF+
Mg2+
AlF+
58
CaAl+
75
FeF+
Mg2+
(Si+)
O+
85
86
88
99
112
Ba+
Li+
OH+
BaF+
Ta
TaO
H+
TaF
H2O+
P+
O2+
a+
TaFO
TaF2
TaO2

Figure 13

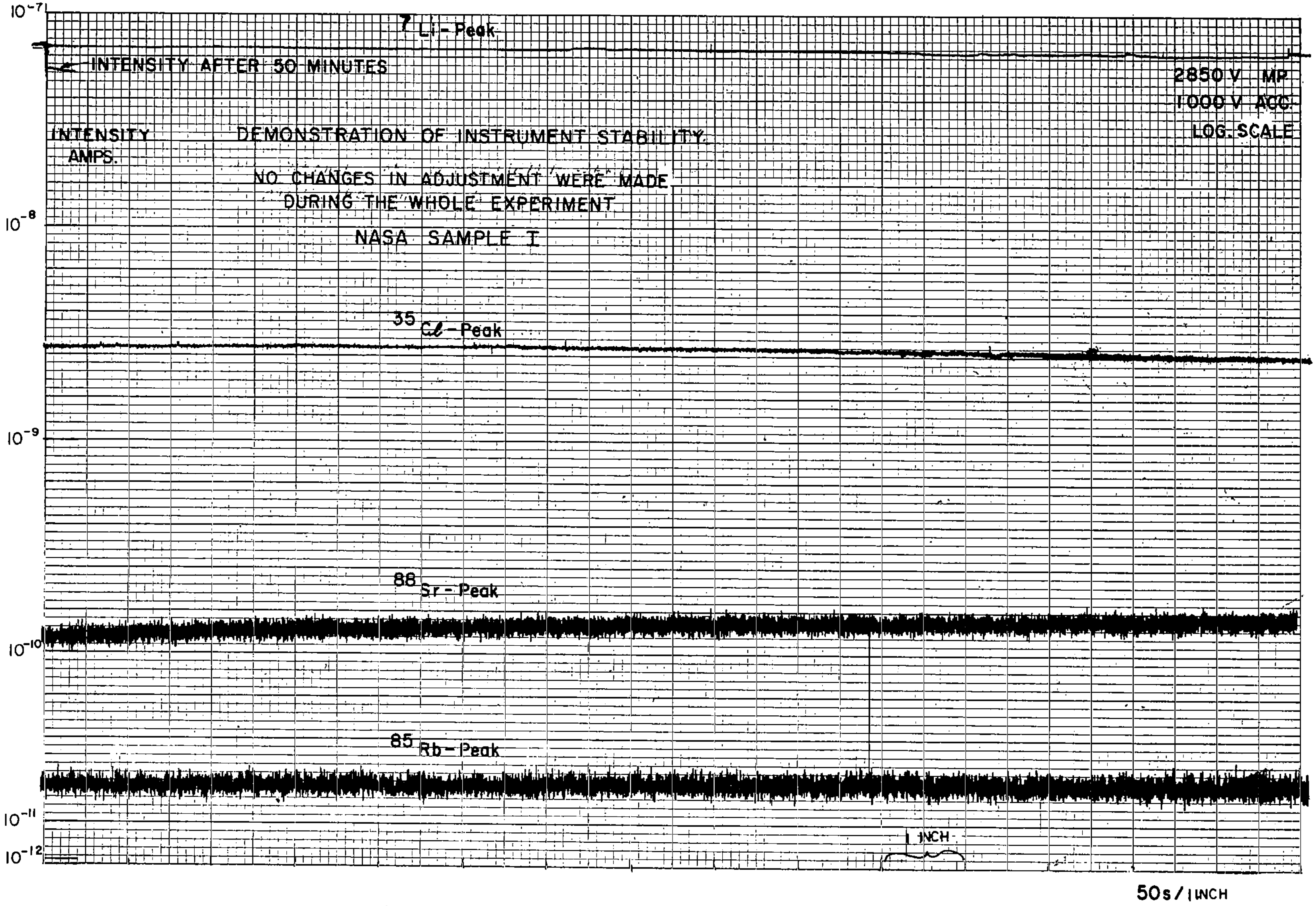
^{7}Li - Peak
INTENSITY AFTER 50 MINUTES
2850 V MP
1000 V ACC.
LOG. SCALE
INTENSITY
AMPS.
DEMONSTRATION OF INSTRUMENT STABILITY
NO CHANGES IN ADJUSTMENT WERE MADE
DURING THE WHOLE EXPERIMENT
NASA SAMPLE I
^{35}Cl - Peak
^{88}Sr - Peak
^{85}Rb - Peak
10^{-7}
10^{-8}
10^{-9}
10^{-10}
10^{-11}
10^{-12}
1 INCH
50s / 1 INCH

Figure 14

could be reached; but the exact potential of the surface was still an unknown factor. The charge-up problem was much more evident with Sample II, and strong fluctuations in the ion current could not be eliminated.

The traces shown in Figure 14 were gained during a total registration time of 50 minutes by bombarding the same spot of the sample without changes in any of the beam adjustment parameters. The statistical noise is increasing with decreasing average signal size, in agreement with theoretical predictions. The drift is a few percent and generally downward, presumably due to cratering of the bombarded spot. Alkali metals sometimes show an initial tendency upward which might be caused by increasing multiplier sensitivity. These metals may form a layer on the first multiplier dynode and increase the secondary electron emission coefficient.

The Measurement of ^{86}Sr/^{88}Sr - On the basis of the good stability obtained with Sample I, the ratio of Strontium 86 to 88 was measured as shown in Figure 15. This measurement was made on the linear scale, sitting alternately on the ^{86}Sr and ^{88}Sr peak. The error caused by drift is reduced by appropriate averaging, as indicated in the figure. Five measurements were made from different points of the sample and yielded the following values:

TABLE I

Number	$\frac{^{86}\text{Sr}}{^{88}\text{Sr}}$	Maximum Deviation Δe	Standard Deviation $\frac{\Sigma\Delta e^2}{n}$	Statistical Error $\frac{\Sigma\Delta e^2}{n(n-1)}$
1	1.099	-0.012	0.006	0.003
2	1.210	-0.020	0.014	0.006
3	1.246	-0.014	0.008	0.003
4	1.173	-0.009	0.006	0.003
5	1.390	+0.009	0.007	0.003

This table shows a clear discrepancy between the results gained from different spots when compared with the reasonably good consistency of the values as long as the same spot was sputtered. Two possibilities could cause these results:

(1) Interference with a molecular ion peak at the two mass numbers 86 and 88.

(2) Inhomogeneity of the sample due to insufficient mixing between the original natural strontium and the added strontium of changed isotopic composition.

The first possibility may be excluded because the examination of spectra with extremely high molecular peaks of this sample gave no indication of a significant interference at these two mass numbers. In addition, all spots used had only small and about equal population of molecular peaks. On the other hand, the spectra gained during the investigation of the rare earths with quasi-controlled charge-up conditions strongly indicated inhomogeneities. This assumption was further supported by an examination of the sputtered sections of the sample under the microscope. The sample showed numerous gas bubbles and differently colored inclusions. Apparently the rock did not completely dissolve in the flux.

Sample II was then compared with Sample I. As already mentioned, stability was a problem with Sample II, but some points of the sample gave a reasonably stable intensity. At present it is not possible to tell whether the signal fluctuations are caused by charge-up effects alone or are due to inhomogeneities in the rather granular structure of this sample. If these fluctuations were purely statistical, the application of the digital memory oscilloscope still should allow intensity ratio measurements of a few percent accuracy.

The spectra of Sample II showed much resemblance with the spectra from Sample I, except that the oxide peaks were substituted by fluorides (Figure 13). The peaks originating from the flux (lithium tetraborate) and due to zirconium oxide (contamination from the crucible) are, of course, absent here.

It was possible to obtain more atomic spectra similar to Sample I. But even in the most favorable cases, there was still an indication of interference at mass 86, supposedly from $CaA\ell F^+$, which obscures the exact $^{88}Sr/^{86}Sr$ ratio. Therefore, no further efforts were undertaken to measure this ratio.

The Rare Earth Region - Sample I shows many lines in the rare earth region (Figure 12). A closer investigation, however, reveals strong interferences with molecular peaks. In some cases, the atomic peaks are completely obscured by oxides, for example, gadolinium is covered by BaO, LaO and CeO. Judging from this spectrum, a direct measurement of isotopic ratios of rare earths in concentrations of a few ppm within such a complex matrix appears as a rather hopeless task. However, the discoveries described in the experimental section above, provide the clue for a possible solution of the problem. The comparison of the spectrum of Figure 12 with others, obtained from the same sample but with obviously different surface charge conditions, indicates that this spectrum was gained from ions with initial energies between 50 and 100 eV. Therefore, molecular species are only slightly suppressed. Some other spectra show the oxide peaks down by almost another order of magnitude, certainly because surface charge conditions allowed the transmission of ions with higher initial energies.

After the new acceleration voltage scanning unit was put in use and the instrument was fitted with the narrow apertures which are necessary for the energy distribution measurements, Sample I was rerun on request of the contract monitor. This time the rare earth region was scanned with the digital memory oscilloscope.

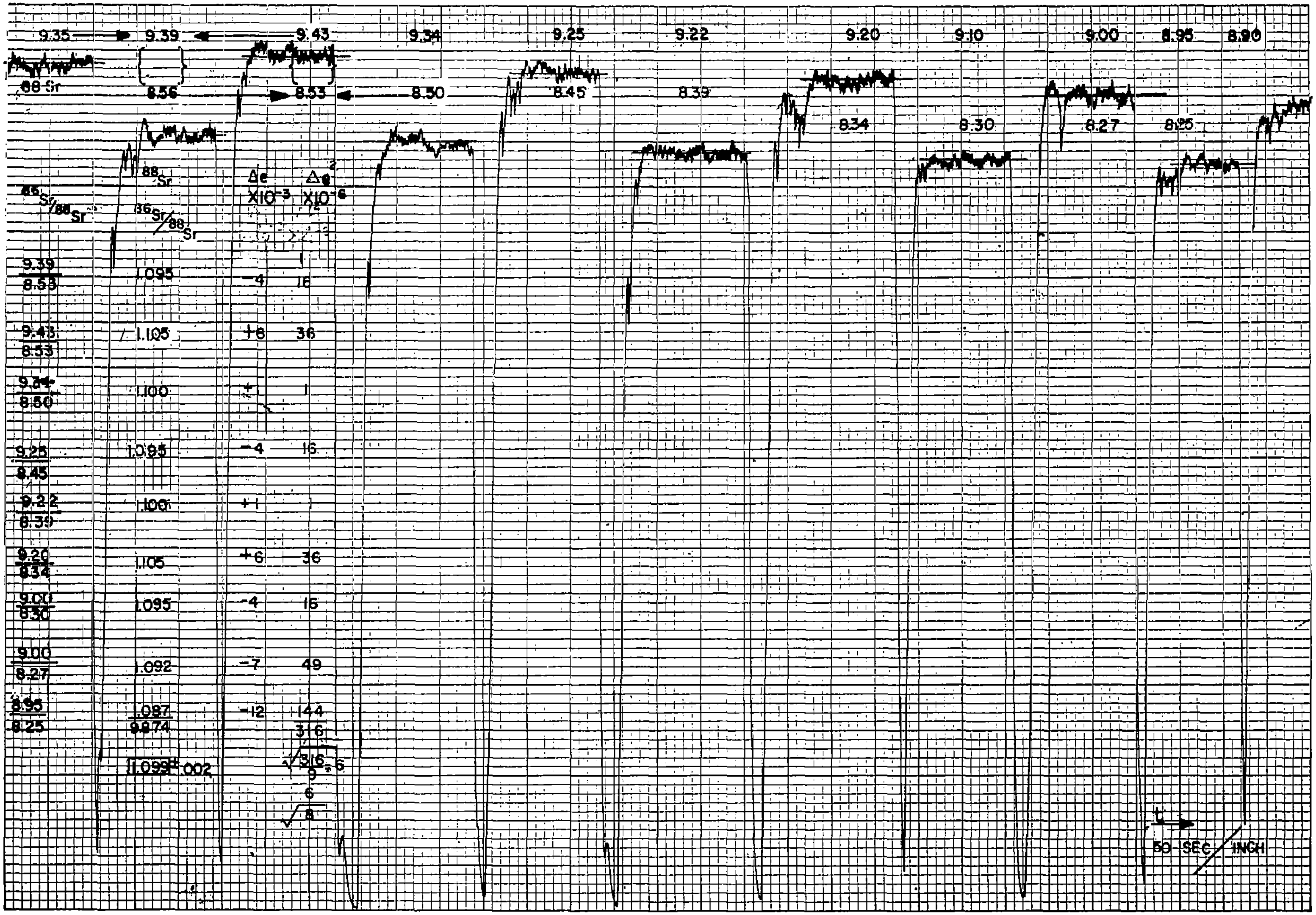

$^{86}Sr/^{88}Sr$	$^{86}Sr/^{88}Sr$	$\Delta e \times 10^{-3}$	$\Delta e^2 \times 10^{-6}$
$\frac{9.39}{8.53}$	1.095	−4	16
$\frac{9.43}{8.53}$	1.105	+6	36
$\frac{9.34}{8.50}$	1.100	+1	1
$\frac{9.25}{8.45}$	1.095	−4	16
$\frac{9.22}{8.39}$	1.100	+1	1
$\frac{9.20}{8.34}$	1.105	+6	36
$\frac{9.00}{8.30}$	1.095	−4	16
$\frac{9.00}{8.27}$	1.092	−7	49
$\frac{8.95}{8.25}$	1.087	−12	144
	9.874		316
	$\boxed{1.099} \pm .002$		$\sqrt{\frac{316}{9}} = 6$
			$\frac{6}{\sqrt{8}}$

Figure 15

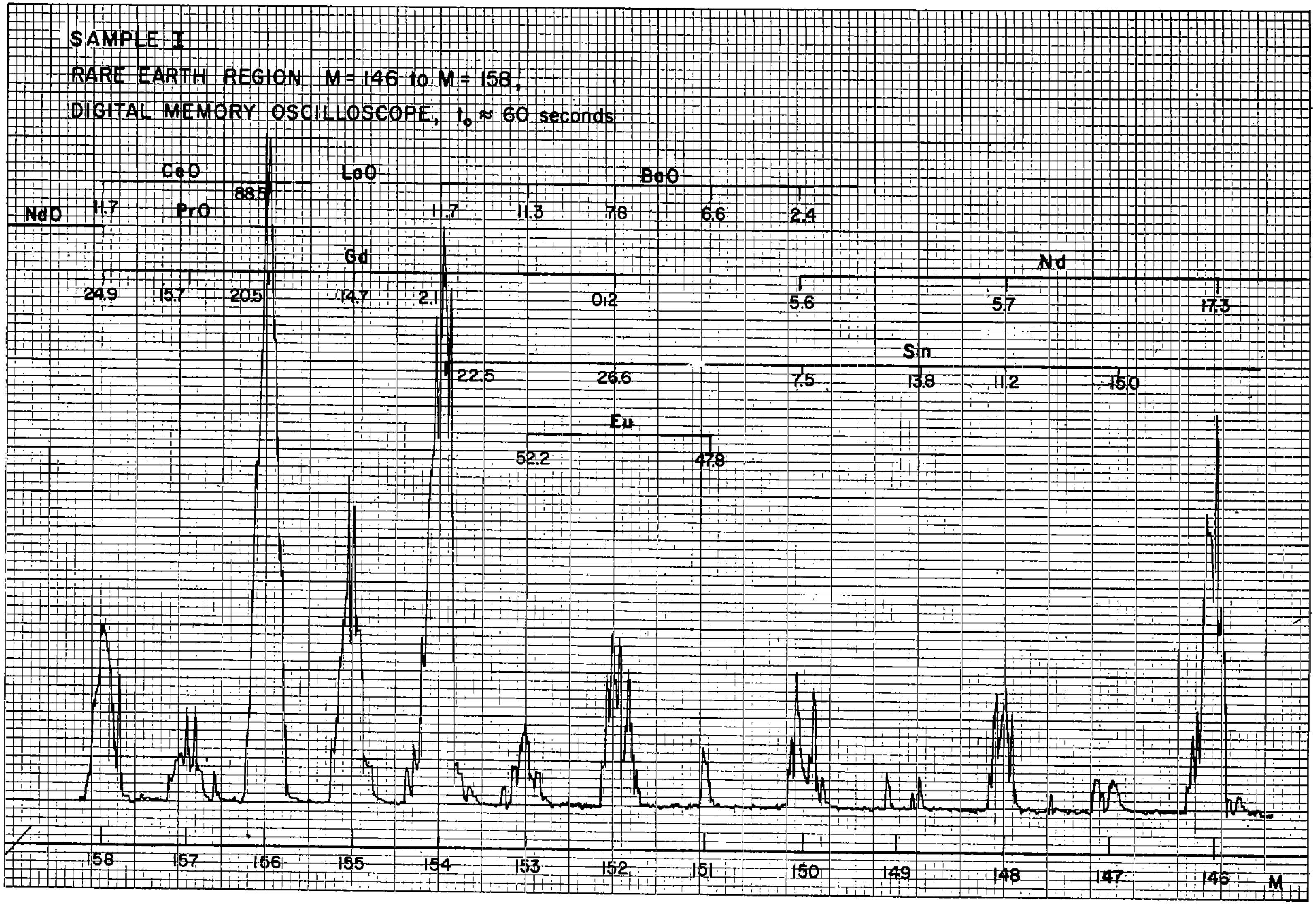
SAMPLE I
RARE EARTH REGION M = 146 to M = 158,
DIGITAL MEMORY OSCILLOSCOPE, $t_0 \approx$ 60 seconds
NdO
11.7
CeO
PrO
88.5
LaO
BaO
11.7
11.3
7.8
6.6
2.4
Gd
24.9
15.7
20.5
14.7
2.1
0.2
Nd
5.6
5.7
17.3
Sm
22.5
26.6
7.5
13.8
11.2
15.0
Eu
52.2
47.8
158
157
156
155
154
153
152
151
150
149
148
147
146
M

Figure 16.

The result for the mass range from 146 to 158 is shown in Figure 16. A rough comparison of the actual peak intensities with those expected for the correct isotope ratios of the rare earth in this range still indicates the strong interferences, mainly from BaO, LaO, and CeO. The peak shapes are considerably distorted by statistical fluctuations, but this is due to the application of a rather short integration time of about 1 minute. No further effort was made to obtain smoother peaks since the obvious interference prohibits meaningful measurements. The same applies for the other sections of the rare earth regions.

However, the following statements have to be made in this connection: The hot filament was not yet available to control surface charge on the sample. Therefore, adjustment of the energy window was not unambiguous. When the acceleration voltage is scanned, as necessary for this measurement, the sample surface potential has to change in a certain proportion, too. This is achieved with a conductive sample simply by scanning the target holder potential. In the case of an insulator and without the discussed hot filament arrangement, however, it is questionable whether the surface potential will follow in the correct relation. If this relation is not maintained, varying energy ranges are transmitted over the scanned mass range.

In addition, the narrow apertures result in a reduction of intensity by a factor of about fifty. Therefore, it was not possible to set the energy window at an energy higher than about 100 eV because the intensity would have been too low for the detection of the rare earths.

Finally, the use of argon ions for the bombardment might not be the best choice. The use of a lighter gas like He might well reduce molecular interferences further. Another interesting alternative lies in the use of H, since the reducing capability of this gas could particularly minimize the oxides.

Evidently more systematical work as described will be necessary to tackle this task more successfully.

SAMPLE PREPARATION

General Aspects

In a number of cases special preparation of a sample is necessary. For the application of isotope dilution techniques, for instance, the original material has to be mixed with a known quantity of one or more enriched isotopes. In the case of solids, the original material either is powderized and mixed with the equally powerized enriched isotopes, or both are dissolved and mixed in the liquid state. The mixed powders or the evaporated residue from the dissolution may be pressed to a compact or preferentially be dissolved into a flux to achieve good homogeneity. The object of the flux is to disperse the sample of interest, such that the aggregates or crystallites of the original materials are eliminated. In this sense, a compact made from evaporated solutions is not as ideal since fractional crystallization occurs, resulting in a heterogeneous dispersion of the species of interest. When such a sample is sputtered, steady intensities and, therefore, correct isotope ratios, are not assured. Regrinding of the diluted and evaporated residue is advised to accomplish a more homogeneous distribution of the elements.

In general, the use of a flux seems to be the more favorable way; however, the composition of the flux has to be selected carefully with respect to the goals of the experiment. Since the fluxing agent introduces a number of elements into the original material, any possible interference with elements in question has to be considered first. This imposes some problems because the flux not only produce atomic peaks, but also molecular species which may comprise elements from the flux and the original material.

In this light, the choice of lithium tetraborate as fluxing agent in a case where Sr, Rb, and the rare earths are of interest is not too fortunate. It is true that the atomic peaks of this flux are far away from the ranges of interest, but the low mass number of Li and B results in a large number of possible molecular species in these ranges if combined with the other main constituents of the sample. Such interferences are very likely because the flux has become one of the major constituents of the sample. The molecular spectra of Sample I clearly show numerous combination peaks of the Li, B and the rock constituents, e.g., Na, B^+, MgB^+, $A\ell B^+$, SiB^+, CaB^+, FeB^+, $FeLi^+$, etc. The chemical reactivity of B seems to enhance particularly such combinations.

An ideal flux has to fulfill two requirements. First, it must dissolve all constituents of the diluted sample; and second, it should only contain elements with masses beyond the mass ranges of interest. More research toward better suited fluxing agents is indicated.

An example for a good fluxing agent which fulfills the first requirement very well but is a compromise as regards the second, was developed by Dr. Nicholls (University of Manchester, England), and successfully used for geo-chemical work. It consists of the following:

SiO_2	49.0%
$A\ell_2O_3$	16.6%
Na_2CO_3	21.7%
K_2CO_3	2.3%
Fe_2O_3	10.4%

All of the above components are available in spectrographic purity, and no elements are introduced which were not already contained in Sample I. Therefore, it was decided to investigate the suitability of this flux for the measurement in the Strontium and rare earth region.

Flux Preparation and Firing

The flux components were obtained from Johnson, Matthey, and Co., Ltd. (Jarrell-Ash distributor) and weighed out accurately in the required amounts. They were then thoroughly ground and mixed. Portions were fired using a gas-oxygen torch. Microscopic examination of the resulting glass first revealed the presence of undissolved particles (probably SiO_2). Further microscopic examination of the mixed and ground starting material showed a fraction of larger crystals which apparently were not dissolved in the firing process.

Consequently, all the material was sieved through a 200 mesh (74μ) SS screen. The residue on the screen was reground and added to what had passed the screen. This was repeated until little residue remained. The screened material was then thoroughly mixed once more, and portions of the powder were pressed into pellets with 1/4 in. diameters. These pellets were fused at $1500^{\circ}C$ with a gas-oxygen torch. The substrate was carbon.

The heating was carried out until bubbling on the surface ceased. A number of pellets were prepared in this way. Several were crushed and the fragments examined under a stereomicroscope for homogeneity. Prior to examination, the fragments were washed and dried to remove very small particles formed in the fragmentation process. The bulk of the material appeared homogeneous and free from bubbles; however, isolated fragments showed regions of translucency of the order of 50 microns. In addition, a surface layer was observed on the pellets which can be attributed to contamination from the torch components. This layer does not create a problem since one can sputter through it to the bulk of the material. A representative pellet was mounted on the target holder of the solids mass spectrometer along with an unfired compressed pellet.

Mass Spectrometric Analysis of Nicholls Glass

The focussed beam was used to obtain spectra of both the unfired and fired flux material. Examination of the data shows the marked improvement in homogeneity resulting from the firing process which apparently has resulted in better mixing. In the unfired material the constancy of the Fe^+/Si^+ ratio indicates that the iron oxide and silica were more homogeneously dispersed than the other components. Otherwise, the spectra of the compact and the fused sample were quite similar with the exception of some enhancement of Na^+ and K^+ in the latter.

Analysis of Nicholls Glass Doped with Strontium

The spectra of the Nicholls flux initially showed no significant lines in the strontium and rare earth region and were well reproducible. Thus, it appeared reasonable to dilute the flux with known quantities of strontium to simulate somewhat the conditions of Sample I to check the accuracy and reproducibility of isotope ratio measurements in such a flux. At first, 1 percent by weight of strontium nitrate was carefully mixed with the powered flux. A portion of this was then diluted with more flux to give a mix containing 0.01 percent by weight of strontium nitrate. Glass spheres were obtained by firing compacted pellets using a gas-oxygen torch. These were analyzed in the solids mass spectrometer. Some of the results are shown in Tables II and III.

TABLE II

INTENSITIES X 10^8 (1 PERCENT Sr IN NICHOLLS GLASS)

O^+	Si^+	K^+	Fe^+	Sr^+	O^+/Si^+	K^+/Si^+	Fe^+/Si^+	Sr^+/Si^+
2.3	105	11.9	16	2.2	0.022	0.11	.15	.021
6.8	97	8.0	13	2.1	0.07	0.082	.13	.022
5.2	83	7.1	12	1.9	0.063	0.086	.14	.023
5.2	73	6.0	11	1.6	0.071	0.082	.15	.022
4.2	71	5.9	11	1.4	0.059	0.083	.15	.020

TABLE III

INTENSITIES X 10^8 (.01 PERCENT Sr IN NICHOLLS GLASS)

O^+	Si^+	K^+	Fe^+	Sr^+	O^+/Si^+	K^+/Si^+	Fe^+/Si^+	Sr^+/Si^+
1.5	69	1.8	9.1	0.016	.022	.026	0.13	.00023
1.2	97	12.8	14.5	0.029	.012	.13	0.15	.00030
1.8	123	10.9	19.0	0.035	.015	.089	0.15	.00028

The Sr^+/Si^+ ratio shows good reproducibility indicating homogeneity. The ratio of the averaged strontium intensities is in fair agreement with the actual concentration ratio of 100. The difference may be due to a non-linear relationship between intensity and concentration in this range, or to the limited accuracy in effecting quantitative transfer, weighing, or to different charge-up conditions.

In addition to studying the constancy of intensities, the strontium isotope ratios were determined in these samples. The results are summarized in Table IV.

TABLE IV

ISOTOPE RATIOS OF STRONTIUM IN A GLASS MATRIX

Wt. % Sr	Sr^{88}/Sr^{86} (exp.)	Sr^{88}/Sr^{86} (lit.)	n	s
1	8.34	8.37	13	0.03
0.01	7.67	8.37	15	0.06
Wt. % Sr	**Sr^{88}/Sr^{87} (exp.)**	**Sr^{88}/Sr^{87} (lit.)**	**n**	**s**
1	12.04	11.78	4	0.097
0.01	11.98	11.78	14	0.067

For the statistical error, the following expression was used:

$$S = \pm\sqrt{\frac{\Sigma(\bar{x} - x_i)^2}{n(n - 1)}}$$

where $\bar{x}$ is the mean value of the ratios, and n is the number of measurements.

The ratio of $^{88}Sr/^{86}Sr$ for the 0.01 percent sample differs significantly from the value of the 1 percent sample, while the ratio of $^{88}Sr/^{87}Sr$ was essentially the same in both samples. Since the original spectra of the flux did not indicate any molecular interference in this range, this deviation was difficult to understand. However, the explanation was found later.

As previously described, the surface charge on the sample can influence the transmitted energy range of the ions in an uncontrolled manner. Thus, the absence of molecular peaks in a certain range may only be due to a condition by which they are suppressed. Obviously, a different charge-up condition prevailed for the analyses of the 0.01 percent strontium sample and resulted in a molecular interference at M = 86. Indeed, a close investigation of the complete spectra of this sample shows enhanced molecular peaks. Later check runs of the Nicholls flux, after the discovery of the energy window phenomena, clearly showed molecular peaks in the strontium range whenever low energy ions were transmitted.

Despite this fact, the Nicholls flux is a better choice than lithium tetraborate. The reasons were already mentioned: It has been used successfully in geological mass spectrometer work, and produces samples of good homogeneity, provided some care in preparation is applied. In addition, and with respect to Sample I, it does not introduce a large quantity of elements into the sample which have not already been there before. The introduction of light elements like Li and B should be avoided in particular because of the manifold combination possibilities which result in a very densely populated molecular spectrum.

The generally complex composition of geological samples will always impose some problems as regards the interference of atomic with molecular peaks. The solution for this problem lies in the possibility of supressing the molecular species; nevertheless, the addition of the flux should not adversely increase the original level of the molecular spectrum.

REFERENCES

1. Poschenrieder, W. P., Herzog, R. F., and Barrington, A. E., "The Relative Abundance of the Lithium Isotopes in the Holbrook Meteorite," Geochimica and Cosmochemica ACTA 29, 1193 (1965).
2. Herzog, R.F.K., Poschenrieder, W. P., Liebl, H. J., and Barrington, A. E., "Solids Mass Spectrometer," NASA Contract NASw-839, GCA Technical Report No. 65-7-N, 47 (1965).
3. Henschke, E. B., "Threshold Energies in Mechanical Collision Theories of Cathode Sputtering," J. Appl. Phys. 33, 1773 (1962).
4. Langberg, E., "Analysis of Low Energy Sputtering," Phys. Rev. 111, 91 (1958).

NASA-Langley, 1967 CR-683